Biogeosciences
Discussions

Biology and air–sea gas exchange controls on the distribution of carbon isotope ratios (δ^{13}C) in the ocean

A. Schmittner[1], N. Gruber[2], A. C. Mix[1], R. M. Key[3], A. Tagliabue[4], and T. K. Westberry[5]

[1]College of Oceanic and Atmospheric Sciences, Oregon State University, Corvallis, Oregon, USA
[2]Institute of Biogeochemistry and Pollutant Dynamics, ETH Zürich, Zürich, Switzerland
[3]Department of Geosciences, Princeton University, Princeton, New Jersey, USA
[4]School of Environmental Sciences, University of Liverpool, Liverpool, UK
[5]Department of Botany and Plant Pathology, Oregon State University, Corvallis, Oregon, USA

Correspondence to: A. Schmittner (aschmitt@coas.oregonstate.edu)

Title Page

Abstract	Introduction
Conclusions	References
Tables	Figures

◄◄	►►
◄	►
Back	Close

Full Screen / Esc

Printer-friendly Version

Interactive Discussion

Abstract

Analysis of observations and sensitivity experiments with a new three-dimensional global model of stable carbon isotope cycling elucidate the processes that control the distribution of δ^{13}C in the contemporary and preindustrial ocean. Biological fractiona-
5 tion dominates the distribution of $\delta^{13}C_{DIC}$ of dissolved inorganic carbon (DIC) due to the sinking of isotopically light δ^{13}C organic matter from the surface into the interior ocean. This process leads to low $\delta^{13}C_{DIC}$ values at dephs and in high latitude surface waters and high values in the upper ocean at low latitudes with maxima in the sub-tropics. Air–sea gas exchange provides an important secondary influence due to two
10 effects. First, it acts to reduce the spatial gradients created by biology. Second, the associated temperature dependent fractionation tends to increase (decrease) $\delta^{13}C_{DIC}$ values of colder (warmer) water, which generates gradients that oppose those arising from biology. Our model results suggest that both effects are similarly important in in-fluencing surface and interior $\delta^{13}C_{DIC}$ distributions. However, air-sea gas exchange is
15 slow, so biological effect dominate spatial $\delta^{13}C_{DIC}$ gradients both in the interior and at the surface, in constrast to conclusions from some previous studies. Analysis of a new synthesis of $\delta^{13}C_{DIC}$ measurements from years 1990 to 2005 is used to quantify pre-formed ($\delta^{13}C_{pre}$) and remineralized ($\delta^{13}C_{rem}$) contributions as well as the effects of bi-ology ($\Delta\delta^{13}C_{bio}$) and air–sea gas exchange ($\delta^{13}C^*$). The model reproduces major fea-
20 tures of the observed large-scale distribution of $\delta^{13}C_{DIC}$, $\delta^{13}C_{pre}$, $\delta^{13}C_{rem}$, $\delta^{13}C^*$, and $\Delta\delta^{13}C_{bio}$. Residual misfits are documented and analyzed. Simulated surface and sub-surface $\delta^{13}C_{DIC}$ are influenced by details of the ecosystem model formulation. For ex-ample, inclusion of a simple parameterization of iron limitation of phytoplankton growth rates and temperature-dependent zooplankton grazing rates improves the agreement
25 with $\delta^{13}C_{DIC}$ observations and satellite estimates of phytoplankton growth rates and biomass, suggesting that δ^{13}C can also be a useful test of ecosystem models.

1   Introduction

The ratio $R = {}^{13}C/{}^{12}C$ of the stable carbon isotopes ^{13}C and ^{12}C in preserved carbonate shells of benthic and planktonic foraminifera is among the most frequently measured quantities from deep-sea sediment core samples. Hence a wealth of data exists on past changes in $^{13}C/^{12}C$ distributions in the ocean (Curry and Oppo, 2005; Sarnthein et al., 2001), typically expressed as the normalized isotopic ratio $\delta^{13}C$:

$$\delta^{13}C = (R/R_{std} - 1) \tag{1}$$

and reported in units of parts per thousand (permil, ‰), where R_{std} is an arbitrary standard ratio, by convention that of the Pee Dee Belemnite, PDB.

Land plants preferentially incorporate ^{12}C relative to ^{13}C into their biomass and typically have $\delta^{13}C$ of about -28‰ for the C_3 photosynthetic pathway and -14‰ for the C_4 pathway (O'Leary, 1988), substantially depleted in ^{13}C relative to the ambient atmosphere (which is -6 to -7‰). Ocean phytoplankton fractionate similarly resulting in typical $\delta^{13}C$ of about -21‰ in bulk marine organic matter compared to a mean surface ocean $\delta^{13}C_{DIC}$ near 2‰. In contrast, calcium carbonate ($CaCO_3$ of corals, benthic shells, or tests of calcareous plankton, i.e. inorganic carbon) has $\delta^{13}C$ relatively close to that of ambient seawater (Turner, 1982) although reconstructions of past oceanic $\delta^{13}C_{DIC}$ from calcareous organisms may be biased by secondary effects such as metabolic rate (Ortiz et al., 1996) and ambient carbonate ion concentration (Spero et al., 1997).

Changes in the global ocean mean of $\delta^{13}C_{DIC}$ in dissolved inorganic carbon (DIC) on geologic timescales ($\geq 10^4$ yr) reflect the balance of erosion and burial of carbonate and organic carbon (Shackleton, 1987; Tschumi et al., 2011; Menviel et al., 2012), while on time scales of up to 10^3–10^4 yr they are generally interpreted as changes in the size and composition of the terrestrial (vegetation and soil) active organic carbon pool (Shackleton, 1977). A reduction of terrestrial organic carbon pool, for example, will lead to a release of CO_2 with low $\delta^{13}C$ into the atmosphere, which will be absorbed

by the ocean on the timescale of decades to centuries. Ultimately the isotopic composition of the atmosphere is controlled by the near-surface seawater isotopic composition, because the ocean contains $> 90\%$ of the actively exchangeable carbon in the ocean-land-atmosphere system (Houghton, 2007). An improved quantification of the processes that control the distribution of carbon isotopes within the ocean as well as ocean-sediment interactions will therefore enable better understanding of long-term sources and sinks of CO_2 (Schmitt et al., 2012).

In paleoceanographic records, the vertical gradients in $\delta^{13}C_{DIC}$ between the warm surface ocean (planktonic foraminifera) and average deep ocean (benthic foraminifera) are generally assumed to reflect the integrated efficiency of the ocean's biological soft-tissue pump (Shackleton et al., 1992; Broecker, 1982; Berger and Vincent, 1986). Variations in spatial gradients of deep-ocean $\delta^{13}C_{DIC}$ are frequently attributed to circulation changes (e.g., Curry and Oppo, 2005) although it has long been known that changes in the preformed properties of paleo-deep water masses are possible (Mix and Fairbanks, 1985; Broecker and Maier-Reimer, 1992; Lynch-Stieglitz and Fairbanks, 1994). Deep-water $\delta^{13}C_{DIC}$ in the contemporary ocean is roughly anti-correlated with nutrient concentrations such as phosphate or nitrate (Broecker and Maier-Reimer, 1992), and with apparent oxygen utilization (AOU) (Kroopnick, 1985). These properties, in turn, reflect differences in preformed properties associated with watermass formation, the accumulation of remineralized organic matter during the time elapsed since isolation from the sea surface, and subsurface mixing between different watermasses (Broecker and Maier-Reimer, 1992). Nutrient concentrations in North Atlantic Deep Water (NADW), for example, are low (with high $\delta^{13}C_{DIC}$) because NADW has recently been sinking from the surface (where nutrients are depleted by phytoplankton), whereas they are high (and $\delta^{13}C_{DIC}$ is low) in Pacific Deep Water (PDW), which is old and has accumulated a large amount of remineralized organic matter. $\delta^{13}C_{DIC}$ and nutrient cycles are linked through phytoplankton growth at the sea surface, which leads to the uptake of inorganic nutrients and isotopically light carbon. This leaves the remaining surface seawater enriched in $\delta^{13}C_{DIC}$ and depleted in nutrients. Upon remineralization at depths, carbon of

Full Screen / Esc

Printer-friendly Version

Interactive Discussion

low δ^{13}C is released proportional to the release of nutrients decreasing δ^{13}C$_{DIC}$ and enriching nutrient concentrations there.

Some of the large changes in δ^{13}C observed for the past, such as during the Last Glacial Maximum (LGM) Atlantic Ocean (Curry and Oppo, 2005; Sarnthein et al., 2001), strongly suggest changed circulation patterns. A recent inverse modeling study showed that, under certain assumptions, the LGM δ^{13}C distribution in the deep Atlantic is inconsistent with the modern flow field (Marchal and Curry, 2008). However, δ^{13}C is in no simple way related to the circulation rate (Legrand and Wunsch, 1995); effects of air–sea gas exchange (Broecker and Maier-Reimer, 1992), variations in the isotopic discrimination during photosynthesis (Goericke and Fry, 1994), and minor buffering by dissolution of calcium carbonate (which has δ^{13}C close to that of seawater) complicate the interpretation of δ^{13}C as a direct nutrient or ventilation proxy. Interpretation of paleo-data on oceanic δ^{13}C is sufficiently complex that a model is needed to deconvolve these various contributions to the record in physically consistent ways.

Here we include ^{13}C cycling directly as prognostic variables in a model of the ocean-atmosphere system, including quantitative descriptions of the fractionation processes. A combination of data and models can then be used to infer the interplay of ocean circulation and isotopic biogeochemistry and to quantify past changes in global ocean carbon cycling. As a first step, such a model needs to be carefully compared to the large amount of existing data from the contemporary ocean, which is an important purpose of this paper. Previous modeling studies have compared different aspects of the simulated ^{13}C cycle with modern observations (Tagliabue and Bopp, 2008; Hofmann et al., 2000; Marchal et al., 1998) but a comprehensive comparison with inorganic and organic carbon isotope measurements has not yet been undertaken. A large number of new measurements that have dramatically increased the data coverage for the modern ocean are now available. Here we present a global compilation of these new measurements of δ^{13}C$_{DIC}$ in dissolved inorganic carbon, analyzed from 1990 to 2005.

We consider three controls on δ^{13}C distribution in the modern (pre-industrial) ocean: (1) biological effects, (2) air–sea gas exchange and (3) the degree of

isotopicdisequilibrium between the surface ocean and the atmosphere, which is longer (∼ 10 yr) than the air–sea equilibration time-scale for CO_2 (∼ 1 yr) (Broecker and Peng, 1982). Previous work has examined some of the important aspects of these processes. Broecker and Maier-Reimer (1992) note that the temperature dependent fractionation during air–sea gas exchange, which leads to lower $\delta^{13}C_{DIC}$ values at higher temperatures, opposes the effect of biological fractionation. However, the temperature effect is moderated by slow air–sea gas exchange. They conclude that for the modern surface ocean the temperature effect largely compensates the biological effect, whereas for the deep ocean the biological effect dominates. These conclusions were confirmed by Lynch-Stieglitz et al. (1995), who analyzed observations and simulations with a model without biology, and Gruber et al. (1999) who analyzed surface observations. Murnane and Sarmiento (2000) (MS00) used a series of model simulations with and without biology and with regular and infinitely fast gas exchange. They concluded that air–sea gas exchange is more important than biology for surface $\delta^{13}C_{DIC}$. No previous study has, to our knowledge, quantified the effects of non fractionating air–sea exchange acting on biologically created gradients or the effect of $CaCO_3$ cycling. Here we present model experiments designed to quantify these effects. A new analysis of observations and model results re-examines the relative importance of biology and gas exchange effects on the $\delta^{13}C_{DIC}$ distribution in the preindustrial and contemporary ocean, given modern physical circulation patterns.

2   Model description

The physical and marine ecosystem models used here are described and validated in detail elsewhere (Schmittner et al., 2008). The three-dimensional ocean general circulation model component of the UVic Earth System Model (Weaver et al., 2001) solves the primitive equations at a relatively coarse spatial resolution (1.8 × 3.6°, 19 vertical levels) and is coupled to a one-layer energy-moisture balance atmospheric model and a dynamic thermodynamic sea ice model. The biogeochemical model includes

interactive nitrogen, phosphorous, oxygen and carbon cycles, but it does not include either silicate or iron (although we include a sensitivity test that addresses potential issues of iron fertilization).

In addition to equations for total carbon ($C = {}^{12}C + {}^{13}C \cong {}^{12}C$), which we assume to approximate ^{12}C since ^{13}C comprises only about 1.1 % of total C and ^{14}C is present only in trace quanities, the isotope ^{13}C has been implemented in all five prognostic carbon variables of the ocean component of the model, that is, in two phytoplankton classes (nitrogen fixers and a general phytoplankton class), zooplankton, detritus and dissolved inorganic carbon (DIC). Fractionation is considered during air–sea gas exchange and during photosynthetic carbon uptake by phytoplankton. In the model $R_{std} = 1$ (Eq. 1) is used in order to minimize numerical errors. Particulate organic matter/carbon (POM/C, detritus) sinks in the model with a depth dependent sinking speed and is remineralized with a linear (first order) constant rate, which leads to an approximately exponential remineralization with an e-folding depth of a few hundred meters. Inorganic carbon ($CaCO_3$), on the other hand, is not simulated as a prognostic variable. $CaCO_3$ production is calculated as a constant fraction of production of POC and instantaneously dissolved in the deep ocean with an e-folding depth of 4 km.

2.1 Air–sea gas exchange

The flux of total $CO_2 = {}^{12}CO_2 + {}^{13}CO_2$ in $mol\,m^{-2}\,s^{-1}$ across the air–sea interface follows the Ocean Carbon Model Intercomparison Project guidelines (Orr et al., 2000)

$$F_C = -k(C_{surf} - C_{sat}), \tag{2}$$

where C_{surf} is the surface aqueous CO_2 concentration, C_{sat} is the saturation concentration corresponding to atmospheric pCO_2, both in $mol\,m^{-3}$, and the piston velocity in $m\,s^{-1}$

$$k = k_0(1 - a_{ice})u^2(Sc/660)^{-0.5} \tag{3}$$

depends on fractional sea ice cover within a grid box, a_ice, wind speed u in m s^{-1}, and the sea–surface temperature (SST in °C) dependent Schmidt number for CO_2, $Sc = 2073.1 - 125.62 \cdot \text{SST} + 3.6276 \cdot \text{SST}^2 - 0.043219 \cdot \text{SST}^3$. Here we use tunable parameter $k_0 = 0.253$ in the default model, which is close to recently updated estimates (0.27) based on radiocarbon (Sweeney et al., 2007; Graven et al., 2012) and 25 % smaller than the value of 0.337 used in previous studies with this model (Schmittner et al., 2008).

The air–sea flux of $^{13}CO_2$ ($F_{^{13}C}$) is calculated according to Zhang et al. (1995):

$$F_{^{13}C} = -k\alpha_k\alpha_{\text{aq}\leftarrow\text{g}}\left(\frac{R_\text{DIC}}{\alpha_{\text{DIC}\leftarrow\text{g}}}C_\text{surf} - R_\text{A}C_\text{sat}\right), \tag{4}$$

The first term in the brackets on the right hand side represents outgassing of oceanic ^{13}C to the atmosphere and is a loss of $^{13}C_\text{DIC}$ from the surface model grid box, and the second term represents invasion of atmospheric ^{13}C into the ocean and is a source of $^{13}C_\text{DIC}$ for the surface model grid box. $\alpha_k = 0.99915$ is a constant kinetic fractionation factor, while $\alpha_{\text{aq}\leftarrow\text{g}} = 0.998764$ is a constant isotopic fractionation factor from gaseous to aqueous CO_2, and

$$\alpha_{\text{DIC}\leftarrow\text{g}} = 1.01051 - 1.05 \times 10^{-4}T \tag{5}$$

is the temperature (in °C) dependent equilibrium fractionation factor from gaseous CO_2 to DIC. Note that $\alpha_{\text{aq}\leftarrow\text{g}}/\alpha_{\text{DIC}\leftarrow\text{g}} = \alpha_{\text{aq}\leftarrow\text{DIC}} \cdot R_\text{DIC} = {^{13}C_\text{DIC}}/({^{12}C_\text{DIC}} + {^{13}C_\text{DIC}})$ is the heavy to total isotope ratio of DIC, $R_\text{A} = {^{13}C_{CO_2}}/({^{12}C_{CO_2}} + {^{13}C_{CO_2}})$ is the heavy to total isotope ratio of atmospheric CO_2.

2.2 Photosynthesis

Isotopic fractionation during photosynthesis is

$$\alpha_{\text{POC}\leftarrow\text{DIC}} = \alpha_{\text{aq}\leftarrow\text{DIC}}\alpha_{\text{POC}\leftarrow\text{aq}} = \frac{\alpha_{\text{aq}\leftarrow\text{g}}}{\alpha_{\text{DIC}\leftarrow\text{g}}}\alpha_{\text{POC}\leftarrow\text{aq}}, \tag{6}$$

where the equilibrium fractionation factor from aqueous CO_2 to particulate organic carbon (POC) depends on the partial pressure of CO_2 in surface water according to Popp et al. (1989)

$$\alpha_{POC \leftarrow aq} = -0.017 \log(C_{surf}) + 1.0034 \tag{7}$$

Initial results with the more process based but more complex formulation based on diffusive CO_2 uptake by phytoplankton from Rau et al. (1996), which considers phytoplankton growth rates and other variables, did not yield better results. This may be due to difficulties of the current model version in simulating the correct phytoplankton growth rates, as a comparison with satellite estimates (Westberry et al., 2008) suggests (Fig. 1). A controversial issue remains to what degree phytoplankton actively acquire CO_2 or bicarbonate, which could affect carbon isotope fractionation differently from a passive, diffusive uptake model (Keller and Morel, 1999).

The effects of biological fractionation of stable carbon isotopes in organic matter are reported as the isotopic enrichment factor

$$\varepsilon = \alpha - 1 \tag{8}$$

Large variations of isotopic enrichment factors have been reported for different phytoplankton species. Diazotrophs (nitrogen fixing microorganisms) in particular appear to show low fractionation factors (Carpenter et al., 1997). Test simulations with a fractionation factor of 12 ‰ for diazotrophs showed small effects (< 0.1 ‰) on the global $\delta^{13}C_{DIC}$ distributions, primarily because of the small direct contribution of diazotrophic organisms to global biomass and primary production. Hence this effect was not included in the default model version.

Fractionation during production of calcium carbonate is small (Turner, 1982) and not considered here (i.e., $\delta^{13}C_{calcite}$ is assumed equal to the $\delta^{13}C_{DIC}$ of the surface watermass where it formed). However, the $CaCO_3$ pump impacts $\delta^{13}C_{DIC}$ by the transport of carbon from the surface to the deep ocean, because calcite dissolves deeper than organic matter, although, as we evaluate below, this effect is small.

3 Sensitivity experiments

We have performed twelve sensitivity experiments (Table 1) designed to quantify the effects of individual processes on the simulated $\delta^{13}C_{DIC}$ distribution (#1–#11) and to illustrates the effect of structural changes in details of the ecosystem model formu-
lation (#12; *FeL*). In addition to the standard full model (*std*; which corresponds to the "OBM" of MS00) simulations without biological fractionation (*no-bio*, $\alpha_{POC\leftarrow DIC} = 1$; which corresponds to the "Solubility Model" of MS00), with only kinetic fractionation (*ki-only*), without gas exchange (*no-gasx*), and without fractionation during air–sea gas exchange (*const-gasx*) are used to quantify the effects of those processes.
 Models *fast-gasx-only*, *bio-fast*, and *fast-gasx* explore the role of much faster gas exchange (twenty times the standard rate for both ^{13}C and total C) alone, with biological fractionation, and with both biological and kinetic fractionation, respectively. (Our experiments *fast-gasx-only* and *fast-gasx* are analogous to the "Potential Solubility Model" to the "Potential OBM" of MS00, respectively.) The fast gas exchange experiments approach the limit of infinitely fast gas exchange, which was determined analytically as $\delta^{13}C_{DIC,inf\text{-}gasx\text{-}only} = 3.9\,‰ - 0.1\,‰(°C)^{-1}\cdot SST$, where $0.1\,‰(°C)^{-1}$ is the slope of the temperature dependence of Eq. (5) and the constant 3.9‰ adjusts the global mean surface $\delta^{13}C_{DIC}$ to be equal to that of model *fast-gasx-only*. Model *no-gasx* has gas exchange of carbon between ocean and atmosphere set to zero. Experiments 9–11 assume different values for a spatially constant biological fractionation factor.
 Experiment 12, *FeL,* uses a simple parameterization of iron limitation of phytoplankton and temperature dependent grazing rates of zooplankton on phytoplankton similar to the independent approach by Keller et al. (2012), who show that these changes improve the seasonality of phytoplankton blooms. Here we use a map of dust fluxes (Mahowald et al., 2005) to scale maximum phytoplankton growth rates and do not limit the increase of zooplankton grazing with temperature above 20°C whereas Keller et al. (2012) used dissolved iron concentrations in sea water simulated by a model with an interactive iron cycle. We acknowledge that dust may not be the only important

source of available iron as a micronutrient (Elrod et al., 2004; Boyd and Ellwood, 2010). Nevertheless, in Fig. 1 we show that this relatively simple addition to the model improves the simulation of phytoplankton growth rates and carbon biomass as judged from a comparison with satellite estimates of these quantities (Westberry et al., 2008). All model simulations were initiated from a 6800 yr long spin up simulation of model *std,* which itself was initiated with δ^{13}C$_{DIC}$ = 0 everywhere, and subsequently integrated for 4000 yr or more (7000 and 8000 yr for *fast-gasx-only* and *ki-only*) with a prescribed pre-industrial value for atmospheric CO$_2$ of δ^{13}C$_A$ = −6.5 ‰ (Francey et al., 1999) until equilibrium was approximated. The last 100 yr of these pre-industrial control simulations are presented in Sect. 5.1.

The anthropogenic release of low δ^{13}C fossil carbon into the atmosphere since the industrial revolution has led to a transient decrease of atmospheric δ^{13}C$_{CO_2}$ by about 1.5 ‰ between pre-industrial background and the year 2000 ("δ^{13}C Suess Effect", Fig. 2); the effect on the surface ocean has been smaller, and spatially variable due to mixing with subsurface watermasses, but still significant. For our simulations of the historical anthropogenic period we use the observed atmospheric CO$_2$ and δ^{13}C$_{CO_2}$ from year 1800 to year 2000 derived from measurements of atmospheric air samples, as well as air samples extracted from Antarctic firn and ice (Allison and Francey, 1999; Francey et al., 1999), as a surface boundary condition (Fig. 2) in addition to climate forcing estimates (Crowley, 2000).

4 Analysis of preformed and remineralized δ^{13}C, effects of biology and air–sea gas exchange

Following previous studies (Kroopnick, 1985; Gruber et al., 1999; Broecker, 1974) it is useful to separate total DIC

$$\text{DIC} \cong {}^{12}\text{C}_{DIC} = {}^{12}\text{C}_{pre} + {}^{12}\text{C}_{org} + {}^{12}\text{C}_{CaCO_3} \tag{9}$$

and ^{13}C

$$^{13}C_{DIC} = {^{13}C_{pre}} + {^{13}C_{org}} + {^{13}C_{CaCO_3}} \tag{10}$$

into preformed components ($^{12}C_{pre}$, $^{13}C_{pre}$) that arise from advection of surface waters with specific $^{12}C_{DIC}$ and $^{13}C_{DIC}$ values into the interior ocean and remineralized components $^{12}C_{rem} = {^{12}C_{org}} + {^{12}C_{CaCO_3}}$ and $^{13}C_{rem} = {^{13}C_{org}} + {^{13}C_{CaCO_3}}$ that arise from the addition of isotopically light carbon from remineralization of organic matter ($\delta^{13}C_{org} \cong -21\,‰$) and isotopically heavy carbon from the dissolution of calcium carbonate ($\delta^{13}C_{CaCO3} \cong 2\,‰$) during the transit time of that water mass. The remineralized organic portions can be approximated as

$$^{12}C_{org} = r_{C:O}AOU \tag{11}$$
$$^{13}C_{org} = R_{org}{^{12}C_{org}}, \tag{12}$$

where $AOU = O_2^{sat} - O_2$ is the Apparent Oxygen Utilization, O_2^{sat} is the temperature and salinity dependent saturation concentration for dissolved oxygen, and R_{org} is the ratio of isotopically heavy over total organic carbon. The inorganic portions are

$$^{12}C_{CaCO_3} = pALK_{dis}/2 \tag{13}$$
$$^{13}C_{CaCO_3} = R_{CaCO_3}{^{12}C_{CaCO_3}}, \tag{14}$$

where $pALK_{dis} = pALK - pALK_{pre}$ is the dissolved portion of the potential alkalinity $pALK = (ALK + NO_3) \cdot 35/S$, i.e. the difference from its preformed value $pALK_{pre}$, and R_{org} is the ratio of isotopically heavy over total $CaCO_3$.

Equations (9) and (10) can be combined to yield

$$\delta^{13}C_{DIC} = \frac{1}{^{12}C_{DIC}}\left(\delta^{13}C_{pre}{^{12}C_{pre}} + \delta^{13}C_{org}{^{12}C_{org}} + \delta^{13}C_{CaCO_3}{^{12}C_{CaCO_3}}\right), \tag{15}$$

which expresses the total $\delta^{13}C_{DIC}$ of a water parcel by the mass-fraction (e.g. $^{12}C_{pre}/^{12}C_{DIC}$) weighted contributions from preformed and remineralized components (Kroopnick, 1985). All terms in Eq. (15) can be estimated except $\delta^{13}C_{pre}$, which we calculate as a residual

$$\delta^{13}C_{pre} = \frac{1}{^{12}C_{pre}} \left(\delta^{13}C_{DIC} \, ^{12}C_{DIC} - \delta^{13}C_{org} \, ^{12}C_{org} - \delta^{13}C_{CaCO_3} \, ^{12}C_{CaCO_3} \right). \tag{16}$$

Similarly $^{12}C_{pre}$ is calculated as the residual from Eq. (9). Note that we use $\delta^{13}C_{org} = -21\,‰$ and $\delta^{13}C_{CaCO_3} = 2\,‰$ for all experiments except for *const-gasx*, for which we use $\delta^{13}C_{org,const\text{-}gasx} = \mathrm{mean}(\delta^{13}C_{detr} \ (z = 0 : 100\,m)) = -29.6\,‰$ and $\delta^{13}C_{CaCO_3,const\text{-}gasx} = \mathrm{mean}(\delta^{13}C_{DIC,const\text{-}gasx} \ (z = 0 : 100\,m)) = -6.5\,‰$, and for *no-bio* and *fast-gasx-only* $\delta^{13}C_{org,no\text{-}bio} = \delta^{13}C_{org,fast\text{-}gasx\text{-}only} = \mathrm{mean}(\delta^{13}C_{DIC} \ (z = 0 : 100\,m)) = 2\,‰$.

Gruber et al. (1999) proposed the following separation into biological and air–sea gas exchange components

$$DIC = C^* + C_{bio} \tag{17}$$

$$^{13}C_{DIC} = \, ^{13}C^* + \, ^{13}C_{bio} \tag{18}$$

where $C_{bio} = C_{soft} + C_{hard}$, $C_{soft} = r_{C:P}\Delta PO_4$, $C_{hard} = \Delta pALK/2$, $^{13}C_{soft} = R_{org}C_{soft}$, and $^{13}C_{hard} = R_{CaCO_3}C_{hard}$, $\Delta PO_4 = PO_4 - PO_4^0$, and $\Delta pALK = pALK - pALK^0$. PO_4^0 and $pALK^0$ are constant reference values. Here we use the global mean surface values. Analogous to Eq. (15) we get

$$\delta^{13}C_{DIC} = \frac{1}{^{12}C_{DIC}} \left(\delta^{13}C^* C^* + \delta^{13}C_{org}C_{soft} + \delta^{13}C_{CaCO_3}C_{hard} \right) \tag{19}$$

Analogous to the calculation of $\delta^{13}C_{pre}$ (Eq. 16) $\delta^{13}C^*$ can be evaluated as the residual. Note that the delta values themselves are not additive. Nevertheless, Gruber

8427

et al. (1999) define the effect of biology as the difference

$$\Delta\delta^{13}C_{bio} \equiv \delta^{13}C_{DIC} - \delta^{13}C^*. \tag{20}$$

We will assess this approximation of biological effects by comparing to our simulation without gas exchange (*no-gasx*), which is only influenced by biology ($\delta^{13}C_{bio} = \delta^{13}C_{DIC,no\text{-}gasx}$).

$\delta^{13}C_{pre}$ and $^{12}C_{pre}$ are related to $\delta^{13}C^*$ and C^* by the following equations:

$$^{12}C_{pre} = C^* + r_{C:P}\Delta PO_{4,pre} + \Delta pALK_{pre}/2 \tag{21}$$

$$\delta^{13}C_{pre} = \frac{1}{^{12}C_{pre}}(\delta^{13}C^*C^* + \delta^{13}C_{org}r_{C:P}\Delta PO_{4,pre} + \delta^{13}C_{CaCO_3}\Delta pALK_{pre}/2), \tag{22}$$

where $\Delta PO_{4,pre} = PO_{4,pre} - PO_{4,pre}^0$ is the difference of the preformed phosphate concentration $PO_{4,pre} = PO_4 - r_{P:O}AOU$ from some reference value $PO_{4,pre}^0$. Here we use the global mean surface phosphate as this reference value. Equations (21) and (22) illustrate that the definitions of $\delta^{13}C^*$ and C^* remove not only the remineralized biological carbon but also the components associated with preformed phosphate and alkalinity.

The effect of air–sea fluxes on surface $\delta^{13}C$ tendencies can be approximated by the difference between the fluxes of ^{13}C (divided by the standard isotopic ratio) and total C:

$$\Delta F_{^{13}C} = F_{^{13}C}/R_{std} - F_C, \tag{23}$$

such that positive values of the difference isotope flux $\Delta F_{^{13}C}$ would tend to increase surface ocean $\delta^{13}C$. Assuming no fractionation during air–sea gas exchange (i.e. all fractionation factors in Eq. (4) are equal to one) and using Eqs. (2) and (4) $\Delta F_{^{13}C}$ becomes

$$\Delta F_{^{13}C,const\text{-}gasx} = -k(\delta^{13}C_{DIC}C_{surf} - \delta^{13}C_A C_{sat}). \tag{24}$$

Equation (24) illustrates that air–sea fluxes will affect surface $\delta^{13}C$ even in the case of no fractionation during air–sea gas exchange if $\delta^{13}C_{DIC}C_{surf} \neq \delta^{13}C_A C_{sat}$. Thus, differences between the surface ocean and atmosphere in either, $\delta^{13}C$, pCO_2, or both, can cause a difference isotope flux. Since biology affects both, it will also influence ΔF_{13_C}.

We will see below that kinetic fractionation has a negligible influence on the $\delta^{13}C$ distribution in the ocean. Similarly the sinking of calcium carbonate has only a minor impact. Therefore these two processes will be neglected in the remainder of the analysis presented in this subsection. In order to separate the effect of biology on air–sea fluxes from those generated by the temperature dependent fractionation we write

$$^{13}C^* = {}^{13}C_{bio}^* + {}^{13}C_T^*, \tag{25}$$

where the temperature dependent part can be further separated into an equilibrium and a disequilibrium part:

$$^{13}C_T^* = {}^{13}C_{T,eq}^* + {}^{13}C_{T,dis}^*. \tag{26}$$

The equilibrium part $^{13}C_{T,eq}^*$ will be the same for all experiments and only depend on temperature, whereas the disequilibrium part $^{13}C_{T,dis}^*$ will depend on the air–sea gas exchange rate such that it is large for slow and small for fast rates. For infinitely fast gas exchange $^{13}C_{T,dis}^* \overset{k_0 \to \infty}{\longrightarrow} 0$.

Distribution of carbon isotope ratios ($\delta^{13}C$) in the ocean

A. Schmittner et al.

Printer-friendly Version

Interactive Discussion

Considering the different effects incorporated in the individual model experiments we write

$$
\begin{aligned}
{}^{13}C_{DIC,std} &= {}^{13}C_{bio} + {}^{13}C^*_{bio,std} + {}^{13}C^*_{T,eq} + {}^{13}C^*_{T,dis,std} \\
{}^{13}C_{DIC,no\text{-}bio} &= \phantom{{}^{13}C_{bio} + {}^{13}C^*_{bio,std} +} {}^{13}C^*_{T,eq} + {}^{13}C^*_{T,dis,std} \\
{}^{13}C_{DIC,fast\text{-}gasx\text{-}only} &= \phantom{{}^{13}C_{bio} + {}^{13}C^*_{bio,std} +} {}^{13}C^*_{T,eq} + {}^{13}C^*_{T,dis,fast} \\
{}^{13}C_{DIC,inf\text{-}gasx\text{-}only} &= \phantom{{}^{13}C_{bio} + {}^{13}C^*_{bio,std} +} {}^{13}C^*_{T,eq} \\
{}^{13}C_{DIC,no\text{-}gasx} &= {}^{13}C_{bio} \\
{}^{13}C_{DIC,cons\text{-}gasx} &= {}^{13}C_{bio} + {}^{13}C^*_{bio,std} \\
{}^{13}C_{DIC,fast-gasx} = {}^{13}C_{DIC,bio\text{-}fast} &= {}^{13}C_{bio} + {}^{13}C^*_{bio,fast} + {}^{13}C^*_{T,eq} + {}^{13}C^*_{T,dis,fast}
\end{aligned}
\tag{27}
$$

This set of Eq. (27) provides a strategy to calculate the individual terms on the right hand side using the sensitivity experiments:

$$
\delta^{13}C^*_{T,dis,fast} \simeq \delta^{13}C^*_{DIC,fast\text{-}gasx\text{-}only} - \delta^{13}C^*_{DIC,inf\text{-}gasx\text{-}only}
\tag{28}
$$

$$
\delta^{13}C^*_{T,dis,std} \simeq \delta^{13}C^*_{DIC,no\text{-}bio} - \delta^{13}C^*_{DIC,inf\text{-}gasx\text{-}only}
\tag{29}
$$

$$
\delta^{13}C^*_{bio,fast} \simeq \delta^{13}C^*_{DIC,bio\text{-}fast} - \delta^{13}C^*_{DIC,no\text{-}bio} - \delta^{13}C^*_{DIC,fast\text{-}gasx\text{-}only} - \Delta\delta^{13}C_{bio}
\tag{30}
$$

$$
\delta^{13}C^*_{bio,std} \simeq \delta^{13}C_{DIC,const\text{-}gasx} - \delta^{13}C_{DIC,no\text{-}gasx}.
\tag{31}
$$

Equations (28)–(31) are approximations assuming that delta values are conserved in addition/subtraction, which, as we have discussed above, is not generally the case. Exact expressions analogous to Eqs. (15), (16), and (19) are not possible since the total carbon expressions corresponding to the individual ${}^{13}C^*$ components are unknown. We will evaluate the errors caused with this assumption for some cases below.

5 Results

Analysis of various sensitivity tests in the pre-industrial model is aimed at separating the influence of different processes and their interactions (Sect. 5.1). This is followed

Full Screen / Esc

Printer-friendly Version

Interactive Discussion

by a detailed comparison of the late 20th century transient simulation of the standard model and model FeL with observations (Sect. 5.2).

5.1 Pre-industrial simulations

5.1.1 Sea surface

Model *std* shows surface values of $\delta^{13}C_{DIC}$ (with $\delta^{13}C_{ATM}$ fixed at −6.5‰) ranging from less than 1‰ around Antarctica up to more than 2.6‰ in the tropics with largest meridional gradients (1.5‰) across the Southern Ocean (Figs. 3 and 4). This pattern is influenced by both biology and air–sea gas exchange. Biological effects ($\delta^{13}C_{bio}$) are well represented by $\Delta\delta^{13}C_{bio}$ estimates, which are consistent for both *std* and *fast-gasx* models with minor differences between the two around Antarctica (Fig. 4, top right panel). They lead to lower values in the Southern Ocean (−2‰), in the subarctic northwest Pacific (−1.5‰), in the Arctic and northern North Atlantic ($\sim$ −0.5‰), and in the tropical regions of upwelling in the eastern parts of the ocean basins ($\sim$ 0.2‰) and higher values in the subtropics ($\sim$ 0.6‰). The areas with relatively low $\delta^{13}C$ are generally associated with regions of incomplete nutrient utilization. Model *FeL* shows somewhat smoother gradients in the tropical Pacific compared with *std* (Fig. 3).

Equilibrium fractionation alone in the case of infinitely fast air–sea gas exchange (*inf-gasx-only*) generates meridional gradients opposing those of biology, due to the temperature dependent fractionation (Eq. 5), which depletes $\delta^{13}C_{DIC}$ by about 1‰ for every 10 °C of warming (Broecker and Maier-Reimer, 1992) and leads to almost 3‰ differences between the equator and high latitudes. Model *fast-gasx-only* approximates that limit, but predicts somewhat smaller meridional gradients due to finite gas exchange, leading to minima of 1.4‰ at low latitudes and maxima of 3.7‰ at high latitudes (Fig. 4, top left panel). However, because of the slow air–sea equilibration time ($\sim$ 10 yr) of surface waters with respect to $\delta^{13}C_{DIC}$ – the surface ocean is nowhere in equilibrium with the atmosphere (Lynch-Stieglitz et al., 1995) – the temperature dependent air–sea gas exchange effect in model *std* ($\delta^{13}C^*_{T,std}$) is much reduced (*no-bio*

versus *fast-gasx-only*) and has less impact on surface ocean $\delta^{13}C_{DIC}$ than biology. The reduced temperature dependent air–sea gas exchange effect in model *std* is also apparent in the larger disequilibrium gradients $\delta^{13}C^*_{T,dis,std}$ compared with $\delta^{13}C^*_{T,dis,fast}$ (Fig. 4, bottom right). The effect of air–sea gas exchange acting on biological gradients in the standard model $\delta^{13}C^*_{bio,std}$ increases $\delta^{13}C_{DIC}$ in the Southern Ocean but has little effects elsewhere (Fig. 4, top right). This effect is more efficient if gas exchange is faster and almost erases the biological gradients in model *fast-gasx*. Meridional gradients of $\sim 1.5\,‰$ created by this effect are amplified by the thermodynamic gradients of $\sim 2.5\,‰$ to result in $> 4\,‰$ gradients created by air–sea gas exchange in model *fast-gasx* ($\delta^{13}C^*_{fast}$, Fig. 4, bottom right). The effect of air–sea gas exchange on surface ocean $\delta^{13}C_{DIC}$ in the standard model ($\delta^{13}C^*_{std}$) is much reduced resulting in meridional gradients of $\sim 1.5\,‰$.

Slow air–sea gas exchange in the standard model leads to biological effects dominating the pre-industrial surface ocean $\delta^{13}C_{DIC}$ distribution. This conclusion is supported by (A) a high positive correlation coefficient ($r = 0.75$) of the spatial (horizontal) variability of surface $\delta^{13}C_{DIC,std}$ with $\Delta\delta^{13}C_{bio}$, whereas the correlation between $\delta^{13}C_{DIC,std}$ and $\delta^{13}C^*_{std}$ is much smaller and negative (-0.35) and (B) smaller spatial (horizontal) variability of $\delta^{13}C^*_{std}$ ($\sigma = 0.61\,‰$) versus that of $\Delta\delta^{13}C_{bio}$ ($\sigma = 0.84\,‰$). Nevertheless, air–sea gas exchange cannot be neglected; it strongly reduces the biologically created gradients ($\Delta\delta^{13}C_{bio}$ vs. $\delta^{13}C_{DIC,std}$).

In the standard model air–sea fluxes (ΔF_{C13}, Fig. 3 top left and Fig. 4 bottom left) tend to increase $\delta^{13}C_{DIC}$ at high latitudes and in the tropics, whereas they tend to decrease $\delta^{13}C_{DIC}$ in the subtropics and at mid-latitudes. Experiments *const-gasx* and *no-bio* both have attenuated fluxes compared with *std* indicating that both biology and fractionation during air–sea gas exchange are similarly important in setting air–sea fluxes in *std*. Fast gas exchange modifies the pattern such that air–sea fluxes north and south of the equator are now acting to strongly decrease surface $\delta^{13}C_{DIC}$, whereas mid-latitude fluxes tend to increase $\delta^{13}C_{DIC}$. The isotopic effects of air–sea fluxes are greatest in

the case with biology and fast gas exchange (*fast-gasx*) because of the larger gradients imposed by biology that are counteracted by gas exchange.

Kinetic fractionation has only a minor effect on surface $\delta^{13}C_{DIC}$ patterns (*ki-only*). At fast gas exchange (*fast-gasx* minus *bio-fast*) kinetic fractionation leads to less than 0.05 ‰ higher values of surface–ocean $\delta^{13}C_{DIC}$ in the eastern equatorial Pacific and Atlantic and variations of less than ±0.01 ‰ elsewhere (not shown).

We conclude that the pre-industrial surface $\delta^{13}C_{DIC}$ patterns are dominated by biology but that they are also markedly influenced by air–sea gas exchange, which decreases the spatial gradients put into place by biology. This is in contrast to the conclusions of Broecker and Maier-Reimer (1992) that the "temperature influence largely compensates" the biological influence and the conclusion by Gruber et al. (1999) that "biological effects on $\delta^{13}C$ nearly offset thermodynamic effects", which were based on the analysis of anthropogenically contaminated observations.

Our conclusion also differs from that of Murnane and Sarmiento (2000) who suggest that the primary factor controlling surface ocean $\delta^{13}C_{DIC}$ distributions is the wind speed dependent gas transfer velocity and that biology is a secondary factor, although their statement refers perhaps more to the potential effect of fast air–sea gas exchange, which can be larger than the biological influence.

As we will show below, the intrusion of isotopically light anthropogenic $\delta^{13}C_{DIC}$ reduces spatial gradients in the surface ocean. Thus transient penetration of anthropogenic carbon into near surface ocean may have lead to the false impression of a compensation between temperature and biological effects, whereas in the preindustrial surface ocean the biological influence may have dominated spatial variability in $\delta^{13}C_{DIC}$ as our model experiments suggest.

5.1.2 Ocean interior

In the plots of vertical distributions of $\delta^{13}C$ (Fig. 5), values from the various model sensitivity tests converge approximately at the sea surface. This is an effect of running the model with a fixed atmospheric $\delta^{13}C$. In the real world, keep in mind that the carbon

Printer-friendly Version

Interactive Discussion

isotope budget of the combined atmosphere-ocean system is largely controlled by the dominant dissolved inorganic carbon reservoir in the deep sea. If the global rather than atmospheric budget of ^{13}C had been fixed, the deep ocean values would approximately converge, and the major divergence between model runs would be in the near-surface ocean and atmosphere.

Model *std* shows nearly constant values of globally horizontally averaged δ^{13}C$_{DIC}$ = 0.5 ‰ below 1 km whereas above that depth δ^{13}C$_{DIC}$ rises rapidly to 2.2 ‰ at the surface (0–100 m) leading to a surface-to-deep gradient of −1.7 ‰ (Fig. 5, top left). About −0.8 ‰ of that gradient in model *std* is caused by the advection of low δ^{13}C$_{pre}$ from high latitudes, particularly from the Southern Ocean, whereas about −0.9 ‰ is due to the remineralization of isotopically light organic matter (δ^{13}C$_{org}$). These contributions correspond to the roughly equal contributions of preformed and remineralized carbon to the deep ocean (Fig. 5, bottom left). The calcium carbonate cycle has only a minor effect and increases deep ocean δ^{13}C$_{DIC}$ by 0.03 ‰ (difference between thick dotted and solid black lines in top left panel of Fig. 5). This effect is small because (a) the smaller relative contribution ($\sim$ 15 %) of the carbonate pump on deep ocean DIC (difference between green and black solid lines in bottom left panel of Fig. 5) and (b) the small difference in δ^{13}C between calcium carbonate and deep ocean DIC (only $\sim$ 1.5 ‰ in contrast to $\sim$ 20 ‰ for organic carbon).

Biological fractionation alone leads to large surface-to-deep gradients of −2.3 ‰ (*no-gasx*, δ^{13}C$_{bio}$, Fig. 5, top), which is slightly underestimated by $\Delta\delta^{13}$C$_{bio}$ (−2.1 ‰). (Nevertheless, $\Delta\delta^{13}$C$_{bio}$ is a good approximation for the three-dimensional distribution of δ^{13}C$_{bio}$ as indicated by their high correlation coefficient of > 0.99.) The potential thermal effect of equilibrium fractionation alone in the case of infinitely fast gas exchange (*inf-gasx-only*; Fig. 5 top left), on the other hand, would lead to 1.6 ‰ higher δ^{13}C$_{DIC}$ values in the deep ocean than at the surface. (Model *fast-gasx-only* approaches that limit, but due to the still finite gas exchange, it predicts a somewhat smaller surface-to-deep δ^{13}C$_{DIC}$ gradient of 1.2 ‰.) Slow air–sea gas exchange, however, limits the thermodynamic effect such that the vertical gradient is reduced to almost 0 ‰ in

experiment *no-bio*, consistent with the results of Murnane and Sarmiento (2000; their "Solubility Model"). Note that changes in air–sea gas exchange do not modulate significantly the impact of remineralized carbon on deep ocean $\delta^{13}C_{DIC}$, which is $\sim 1\,‰$ in all cases with biological fractionation (differences between dashed and corresponding solid lines in top left panel of Fig. 5).

Model *const-gasx* as well as the difference *std – no-bio* (green line in top right panel of Fig. 5) display consistently slightly smaller vertical gradients than $\delta^{13}C_{bio}$ and $\Delta\delta^{13}C_{bio}$ indicating the small but significant (0.1–0.5 ‰) moderating effect of non-fractionating gas exchange on biologically created vertical gradients ($\delta^{13}C^*_{bio,std}$). This non-fractionating gas exchange effect is stronger ($\sim 0.7\,‰$) in the case of fast gas exchange ($\delta^{13}C^*_{bio,fast}$) and conspires with the reduced disequilibrium thermodynamic effect $\delta^{13}C^*_{T,dis,fast}$ (bottom right panel of Fig. 5) to generate small vertical gradients in model *fast-gasx* (top left panel, Fig. 5).

In model *std*, however, the disequilibrium thermodynamic effect cancels almost entirely the equilibrium thermodynamic effect (black and green lines in bottom right panel of Fig. 5). Together with the small effect of $\delta^{13}C^*_{bio,std}$ this causes the overall effect of air–sea gas exchange to increase deep ocean values by $\sim 0.3\,‰$ with respect to the surface ($\delta^{13}C^*_{std}$). Fast gas exchange, in contrast, increases deep ocean values by more than 2 ‰ with respect to the surface ($\delta^{13}C^*_{fast}$).

The effects of kinetic fractionation (*ki-only*) on deep ocean $\delta^{13}C_{DIC}$ are negligibly small.

In model *fast-gasx-only*, although biological fractionation is zero, the sinking of organic matter and calcium carbonate delivers the surface $\delta^{13}C_{DIC}$ signature to the deep ocean, reducing vertical gradients by 0.1 ‰ (dashed vs solid blue lines in top left panel of Fig. 5). This effect is weaker in model *no-bio* since vertical gradients in $\delta^{13}C_{DIC}$ are weaker.

In model *std* zonally averaged preindustrial $\delta^{13}C_{DIC}$ in the deep ocean varies from 1.6 ‰ in the North Atlantic to −0.2 ‰ in the North Pacific (Fig. 6). The spatial variability

in the deep ocean is dominated by 2.0‰ variations of $\Delta\delta^{13}C_{bio}$, decreasing from −0.7‰ in the North Atlantic to −2.7‰ in the North Pacific, whereas $\delta^{13}C^*$ variations are smaller (0.5‰) and increase from 2.2‰ in the North Atlantic to 2.7‰ in the Southern Ocean. A pronounced maximum of $\delta^{13}C^*$ is simulated in Antarctic Inter-

5 mediate Water (AAIW) in the Atlantic with values ranging from 3‰ at high latitudes to ∼ 2.4‰ in the tropics, consistent with estimates based on observations (Charles et al., 1993). Remineralized isotope signature ($\Delta\delta^{13}C_{rem} = \delta^{13}C_{DIC} - \delta^{13}C_{pre}$) variations are similar to those of $\Delta\delta^{13}C_{bio}$ except in the Atlantic, where they are smaller, whereas absolute values of $\Delta\delta^{13}C_{rem}$ are higher than $\Delta\delta^{13}C_{bio}$. Most of the differences between

10 $\Delta\delta^{13}C_{bio}$ and $\Delta\delta^{13}C_{rem}$ (and between $\delta^{13}C^*$ and $\delta^{13}C_{pre}$) can be explained by preformed nutrients, which are higher in Southern Ocean deep and intermediate water masses and lower in North Atlantic Deep Water (NADW) and exhibit larger variability in the deep Atlantic compared to the Indo-Pacific (Ito and Follows, 2005; Schmittner and Galbraith, 2008). $\delta^{13}C_{pre}$ variations are much smaller and decrease by ∼ 0.4‰

15 from the North Atlantic towards the North Pacific. In the thermocline the variability of $\delta^{13}C_{pre}$ is larger (1‰), reflecting more the surface variations (Fig. 3).

Individual contributions to $\delta^{13}C^*$ are shown in Fig. 7. By definition $\delta^{13}C^*_{T,eq}$ depends only on temperature and varies from ∼ 1‰ in the tropical surface ocean to ∼ 3.8‰ in the abyss and high latitude surface waters. Due to large disequilibrium

20 effects caused by the slow air–sea gas exchange these variations are only weakly expressed in $\delta^{13}C^*_{T,std}$, which shows minima of ∼ 1.6‰ in subtropical surface waters and maxima of ∼ 2.7‰ in surface waters of the Southern Ocean and northwest Pacific (not shown) and small variations (∼ 0.2‰) in the deep ocean. The non-fractionating effect of air–sea gas exchange acting on the biological gradients ($\delta^{13}C^*_{bio,std}$) leads

25 to minima in the subtropical surface and maxima in AAIW and Antarctic Bottom Water (AABW). Thus the maximum in $\delta^{13}C^*$ in AAIW is caused in approximately equal parts by $\delta^{13}C^*_{T,std}$ and $\delta^{13}C^*_{bio,std}$. It is interesting to note that for fast gas exchange

Distribution of carbon isotope ratios ($\delta^{13}C$) in the ocean

A. Schmittner et al.

Full Screen / Esc

Printer-friendly Version

Interactive Discussion

the AAIW maximum in $\delta^{13}C^*_{T,fast}$ is less pronounced than $\delta^{13}C^*_{T,std}$, whereas it is more pronounced in $\delta^{13}C^*_{bio,fast}$.

We conclude from these preindustrial simulations that the vertical distribution of $\delta^{13}C_{DIC}$ in the ocean and the spatial gradients between deep water masses are dominated by the effects of biological fractionation, in agreement with previous studies (Broecker and Maier-Reimer, 1992; Lynch-Stieglitz et al., 1995; Murnane and Sarmiento, 2000). Air–sea gas exchange reduces the $\delta^{13}C_{DIC}$ gradients generated by biology by 10–20 % in the pre-anthropogenic simulation. Under different climate regimes this fraction as well as the efficiency of gas exchange as a means of changing the preformed properties of watermasses entering the ocean interior could be different.

5.2 Present day (1990–2005) observations and simulations

The modeled large-scale circulation and distribution of biogeochemical tracers is generally in good agreement with observations, although systematic biases remain. In the North Pacific, stratification is too weak leading to anomalously high subsurface oxygen and low DIC and nutrient concentrations there. In the deep Indian Ocean, oxygen and radiocarbon are too high while DIC and nutrient concentrations are too low (Schmittner et al., 2008). The model does not include interactive iron and silicon cycles, which leads to biases in simulating phytoplankton growth rates. These known biases also affect the simulated $\delta^{13}C_{DIC}$ distribution, which we need to consider when comparing model results to observations. In this section annual mean values will be used for all data unless specified otherwise.

5.2.1 Particulate organic matter

Figure 8 compares model results to the compilation of measurements of $\delta^{13}C$ in particulate organic matter (POM) in the near surface ocean by Goericke and Fry (1994). Particulate organic carbon is about 2 ‰ lower in the 1990s compared with the preindustrial simulation due to both the decrease of surface-ocean $\delta^{13}C_{DIC}$ and an increase

Full Screen / Esc

Printer-friendly Version

Interactive Discussion

in the pCO$_2$-dependent fractionation (Eq. 7). Models *FeL* and *std* simulate very similar zonally averaged δ^{13}C$_{POC}$ distributions. Both reproduce the observed general meridional gradient of δ^{13}C$_{POC}$ with less negative values of about −20 ‰ at low latitudes and more negative values (−25 to −30 ‰) at high latitudes, similar to earlier studies (Hofmann et al., 2000; Murnane and Sarmiento, 2000). Correlation coefficients between model results and observations of $r = 0.74$ (*FeL*), $r = 0.71$ (*std*) and normalized (by the standard deviation of the observations, which is $\sigma_{obs} = 2.8$ ‰) root mean squared errors are NRMSE = 0.92 (*FeL*) and NRMSE = 0.98 (*std*) suggest model *FeL* is in slightly better agreement with the observations than model *std*.

However, closer inspection reveals that model *FeL* underestimates δ^{13}C$_{POC}$ in the eastern tropical Pacific (a bias that is exacerbated in model *std*; not shown), in the subarctic North Pacific and in the high-latitude North Atlantic. It is unable to reproduce the pronounced interhemispheric difference at mid to high latitudes apparent in the observations; qualitatively similar biases occurred in the more complex model of Tagliabue and Bopp (2008).

Large gaps in the data coverage hamper a more comprehensive model validation at this time. An updated compilation of surface δ^{13}C$_{POC}$ measurements and new measurements, particularly in the Pacific, are urgently required to improve the validation of biological fractionation in global models. Surface sediment data may provide an alternative to sea surface δ^{13}C$_{POC}$ measurements, a possibility that should be explored in the future.

Future improvements of the model will need to include a more realistic treatment of biological fractionation such as outlined in the approaches of Rau et al. (1996) and Keller and Morel (1999). This will likely require more ecosystem and nutrient information to constrain the relative growth rates and isotopic fractionation of different classes of plankton.

5.2.2 Surface dissolved inorganic carbon

The global mean surface $\delta^{13}C_{DIC}$ value from the 1990–2005 observations of 1.5 ‰ is in good agreement with model *FeL*. Model *std*, however, overestimates mean surface $\delta^{13}C_{DIC}$ by 0.2 ‰ mainly due to a bias in the tropics (Figs. 3, 9). As noted earlier by Gruber et al. (1999) observations show that $\delta^{13}C_{DIC}$ is relatively constant over most of the surface ocean; zonally averaged values range between 1 and 2 ‰, although the total range of measured $\delta^{13}C_{DIC}$ values stretches between 0.5 and 2.4 ‰. Larger simulated latitudindal gradients in surface-ocean $\delta^{13}C_{DIC}$ for preindustrial time (1–2.5 ‰ for zonally averaged values; Fig. 4) suggest that the measured gradients are reduced as a result of the accumulation of anthropogenic carbon into the tropical and subtropical oceans. Anthropogenic carbon reduces the area-weighted spatial (horizontal) standard deviation of surface $\delta^{13}C_{DIC}$ from 0.37 ‰ at year 1800 to 0.27 ‰ at year 2000 in model *FeL*. The reduction in spatial variability is almost identical (0.36 ‰ in 1800 to 0.27 ‰ in 2000) in model *std*.

High surface $\delta^{13}C_{DIC}$ values are observed in the western equatorial Pacific, in the central Pacific south of the equator, in the southeast Pacific, in the tropical Atlantic and near the subantarctic front in the Southern Ocean. Low values are found in the Indian Ocean, the northeast Pacific, the central and eastern equatorial Pacific, the northwestern subtropical Pacific, the subtropical North Atlantic as well as at high latitudes. Model *FeL* captures many of the observed spatial patterns of surface ocean $\delta^{13}C_{DIC}$ with a correlation coefficient of $r = 0.53$ and NRMSE = 0.99. Zonally averaged $\delta^{13}C_{DIC}$ values in model *FeL* are generally consistent with observations except around 20° N and in the Arctic, where the model is biased high. However, model *std* ($r = 0.49$; NRMSE = 1.19) overestimates $\delta^{13}C_{DIC}$ in the tropics (by up to 0.4 ‰ and for the zonal average by 0.2–0.3 ‰) except for the eastern equatorial Pacific where $\delta^{13}C_{DIC}$ is underestimated (not shown, but see Fig. 3 for the differences with model *FeL* in preindustrial patterns). Including iron limitation reduces phytoplankton growth rates, carbon biomass, and hence primary productivity in the eastern equatorial Pacific (Fig. 1) and

eliminates the bias in $\delta^{13}C_{DIC}$. This illustrates the importance of details of ecosystem model dynamics on the $\delta^{13}C$ distribution and suggests that $\delta^{13}C$ observations can help evaluate ocean ecosystem models.

Remaining biases in model *FeL* include overestimated surface-ocean $\delta^{13}C_{DIC}$ values in parts of the tropical Atlantic and Indian Ocean, along 20° N in the North Pacific, in the northern North Pacific and northern North Atlantic, and in the mid latitude South Atlantic as well as underestimation of surface-ocean $\delta^{13}C_{DIC}$ in the Southern Ocean and eastern tropical Pacific.

The model suggests that pre-industrial $\delta^{13}C_{DIC}$ values at the sea surface were, on a global average, 2.3 ‰, or 0.67 ‰ higher than in the 1990's in agreement with the previous estimates by Broecker and Maier-Reimer (1992) and Sonnerup et al. (2007, 0.76 ± 0.12 ‰). Ortiz et al. (2000) calculated a shift of 0.62 ± 0.17 ‰ in the Northeast Pacific (using data from 1991), consistent with the model 1980–2000 mean between 138° W to 120° W and 28° N to 45° N of 0.75 ‰. Surface-ocean $\delta^{13}C_{DIC}$ decreases faster in the subtropics than at other latitudes consistent with previous analysis of observations (Quay et al., 2003). Between the 1980s and the 1990s its decrease ranges from minima of ∼ 0.04 ‰ at high latitudes to 0.2 ‰ in the subtropics, and ∼ 0.14 ‰ in the tropics, consistent with previous studies (e.g. Gruber et al., 1999).

5.2.3 Ocean interior dissolved inorganic carbon

Spatial gradients in deep water $\delta^{13}C_{DIC}$ of about 1.6 ‰ are apparent between different ocean basins in both observations and in the model (Figs. 10, 11). Highest values of around 1 ‰ are found in the North Atlantic, whereas lowest values of less than −0.6 ‰ are found in the North Pacific at about 1 km depth, consistent with an earlier data compilation (Kroopnick, 1985). The model captures the three-dimensional distribution as indicated by a correlation coefficient of $r = 0.88$ and NRMSE = 0.50 ($\sigma_{obs} = 0.48$ ‰). The model results are, however, biased high by 0.08 ‰. A high bias is not uncommon. For example, Sonnerup and Quay (2012) tested several models all of which were

Full Screen / Esc

Printer-friendly Version

Interactive Discussion

biased high by 0.13–0.51‰. Similarly the Tagliabue and Bopp (2008) models were also all high biased (e.g. below 1 km depth all were more than 0.45‰ too high) but the numbers cannot be precisely compared with ours because they did not present volume weighted averages and used a much sparser dataset.

Isolating the biological, remineralized, preformed, and gas exchange components shows that most of the observed variability of $\delta^{13}C_{DIC}$ in the deep ocean is due to $\Delta\delta^{13}C_{bio}$ (Fig. 10), which ranges from values close to -1‰ in the North Atlantic to -2.8‰ in the North Pacific. Much of this variability is due to the effect of remineralized matter $\Delta\delta^{13}C_{rem}$, which ranges from -0.3‰ in the North Atlantic to -1.7‰ in the North Pacific. Observed $\delta^{13}C_{pre}$ shows little variability in the deep ocean but maxima in the thermocline in all ocean basins, particularly at low latitudes. Model results reproduce this pattern (Fig. 11) and indicate that large vertical gradients in preindustrial $\delta^{13}C_{pre}$ in the upper thermocline have been reduced due to the invasion of anthropogenic carbon (Fig. 11 vs. Figs. 6 and 13). Higher preformed values of upper ocean and intermediate waters are consistent with the simulated preindustrial surface $\delta^{13}C_{DIC}$ distribution (Fig. 3), which shows lower values at high latitude regions of deep water formation and higher values in lower latitude regions of intermediate and mode water formation. For preindustrial times the model simulates a monotonic decrease of $\delta^{13}C_{pre}$ from the surface down (Fig. 6). Thus, the intermediate depth maximum simulated for the contemporary ocean is caused by the downward penetration of light carbon from above superimposed on this background gradient, suggesting that this is also the reason for the observed pattern.

The spatial gradients in observed $\delta^{13}C^*$ are larger than those for $\delta^{13}C_{pre}$ and show minima in the subtropical surface ocean of ~ 1‰ and maxima of up to 3‰ for AAIW. Pronounced differences are apparent between water masses of southern origin, which are high in $\delta^{13}C^*$ and NADW, which has lower values. Models *FeL* and *std* reproduce the general patterns found in the observations, but they underestimate the AAIW maximum (Fig. 12). Preindustrial model results show much reduced vertical gradients of

Distribution of carbon isotope ratios ($\delta^{13}C$) in the ocean

A. Schmittner et al.

Title Page

Abstract | Introduction

Conclusions | References

Tables | Figures

◀ | ▶

◀ | ▶

Back | Close

Full Screen / Esc

Printer-friendly Version

Interactive Discussion

$\delta^{13}C^*$ in the thermocline (Fig. 6) indicating that the large gradients in the contemporary observations are partly caused by anthropogenic carbon.

The latitudinal distribution of the simulated anthropogenic $\delta^{13}C_{DIC}$ shift in the North Pacific is consistent with the data based multi-parameter mixing model of Sonnerup et al. (2007), who found surface values ranging from 0.8 ‰ in the subtropics to 0.2–0.4 ‰ poleward of 40° N and vertical integrated values to be −200 ‰ m at high latitudes and −400 to −500 ‰ m at low latitudes. Along 165° E model FeL predicts for the 1990s −280 ‰ m around 45° N and −430 ‰ m at 30° N.

6 Summary and conclusions

Comparison of a new three-dimensional model of ^{13}C cycling in the ocean with a new global database of $\delta^{13}C_{DIC}$ observations shows broad agreement in important large-scale features such as the vertical and inter-basin gradients. Our results support earlier findings suggesting that effects of biological fractionation dominate the interior $\delta^{13}C_{DIC}$ distribution in the modern and pre-anthropogenic ocean, whereas the effect of air–sea gas exchange is to reduce the biologically-imposed $\delta^{13}C_{DIC}$ gradients (Murnane and Sarmiento, 2000; Lynch-Stieglitz et al., 1995; Broecker and Maier-Reimer, 1992; Kroopnick, 1985). In contrast to previous studies that have attributed the effect of air–sea gas exchange only or mainly to the temperature dependent fractionation (Charles et al., 1993; Broecker and Maier-Reimer, 1992; Lynch-Stieglitz et al., 1995; Murnane and Sarmiento, 2000) we have shown that temperature independent air–sea fluxes acting only on biologically created gradients are equally important.

In contrast to previous conclusions (Gruber et al., 1999; Broecker and Maier-Reimer, 1992; Lynch-Stieglitz et al., 1995) that biological and air–sea gas exchange influences nearly cancel for surface $\delta^{13}C_{DIC}$ distributions, we find that the air–sea gas exchange, although acting to reduce the biological effect, is not able to cancel it for preindustrial times. Our model results suggest that the uptake of anthropogenic carbon has reduced the spatial gradients in $\delta^{13}C_{DIC}$ that were present in the preindustrial surface ocean.

The anthropogenic overprint is largest in the subtropics (Fig. 13), where it reduces the preindustrial δ^{13}C$_{\text{DIC}}$ maximum (Figs. 3, 8). This may explain the different conclusions on the relative strength of biological vs gas exchange effects on δ^{13}C reached previously based on analyzed observations affected by anthropogenic carbon (Gruber et al., 1999; Broecker and Maier-Reimer, 1992). Although the gas exchange effects are relatively minor in today's (modern and pre-anthropogenic) oceans, our model sensitivity tests suggest that changes in gas exchange rate could potentially be and important mechanism for changing the iosotpic budget of the ocean interior in a different climate.

The model data comparison revealed a number of important model deficiencies, such as modeled δ^{13}C$_{\text{DIC}}$ values being too high in the deep ocean, particularly the North Atlantic, Indian and North Pacific. Decomposition into the different components and effects may help in improving the model in the future, e.g. by improving AOU and/or preformed nutrient distributions. The model may be a useful tool for paleoclimate and other applications.

Appendix A

Observations

The primary data source for the δ^{13}C$_{\text{DIC}}$ measurements is the Web Accessible Visualization and Extraction System (W.A.V.E.S) at the Carbon Dioxide Information Analysis Center (CDIAC) (http://cdiac3.ornl.gov/waves/discrete/). On 27 August 2010 we extracted data from two databases within CDIAC: First, from the Global Data Analysis Project GLODAP (Key et al., 2004) and second, from the **Car**bon Dioxide **in** the **A**tlantic Ocean (CARINA) data synthesis project mainly from WOCE and CLIVAR expeditions.

The δ^{13}C$_{\text{DIC}}$ data on file at CDIAC have not been quality controlled. In the GLODAP database, some cruises (for example, 316N145_5 and INDIGO 123) had obvious bad data, and these were excluded from our compilation. From the remaining 31 GLODAP expeditions, we removed bottle numbers > 70 from seven cruises in order to

exclude large volume (LV) samples, many of which had large negative biases. From the CARINA database cruise 64TR19900417 was excluded due to obvious bad data, leaving 18 cruises. The remaining combined GLODAP and CARINA database contains 17 989 δ^{13}C$_{DIC}$ data for the time period from 1990–2005 from all oceans and all depths. These data were supplemented by 632 measurements from 1990 to 1998 made at Charles (Dave) Keeling's laboratory at Scripps Institution of Oceanography, described by Gruber et al. (1999), and by one transect (50 data points) from the northeast Pacific measured in Alan Mix's laboratory at Oregon State University, published along with nutrient data by (Ortiz et al., 2000). The Keeling dataset is also available at CDIAC (http://cdiac.ornl.gov/ftp/oceans/keeling.data/), although here we used one single data file provided by N. Gruber. We do not use measurements prior to 1990 (such as all GEOSECS and TTO data). Due to unresolved calibration issues the accuracy is currently estimated to be 0.1–0.2 ‰ (A. McNichol, personal communication, 2012). The combined data set contains a total of 18 670 δ^{13}C$_{DIC}$ measurements. It is freely available at http://people.oregonstate.edu/~schmita2/data/schmittner13bg.

References

Berger, W. H. and Vincent, E.: Deep-sea carbonates – reading the carbon-isotope signal, Geol. Rundsch., 75, 249–269, 1986.

Boyd, P. W. and Ellwood, M. J.: The biogeochemical cycle or iron in the ocean, Nat. Geosci., 3, 675–682, 2010.

Broecker, W. S.: "NO" a conservative water-mass tracer, Earth Planet. Sc. Lett., 23, 100–107, 1974.

Broecker, W. S.: Ocean chemistry during glacial time, Geochim. Cosmochim. Ac., 46, 1689–1705, 1982.

Broecker, W. S. and Maier-Reimer, E.: The influence of air and sea exchange on the carbon isotope distribution in the sea, Global Biogeochem. Cy., 6, 315–320, doi:10.1029/92gb01672, 1992.

Broecker, W. S. and Peng, T. H.: Tracers in the Sea, Eldigio, Palisades, New York, 1982.

Carpenter, E. J., Harvey, H. R., Fry, B., and Capone, D. G.: Biogeochemical tracers of the marine cyanobacterium Trichodesmium, Deep-Sea Res. Pt. I, 44, 27–38, 1997.

Charles, C. D., Wright, J. D., and Fairbanks, R. G.: Thermodynamic influences on the marine carbon isotope record, Paleoceanography, 8, 691–697, doi:10.1029/93PA01803, 1993.

Crowley, T. J.: Causes of climate change over the past 1000 years, Science, 289, 270–277, 2000.

Curry, W. B. and Oppo, D. W.: Glacial water mass geometry and the distribution of delta C-13 of Sigma CO2 in the western Atlantic Ocean, Paleoceanography, 20, PA1017, doi:10.1029/2004PA001021, 2005.

Elrod, V. A., Berelson, W. M., Coale, K. H., and Johnson, K. S.: The flux of iron from continental shelf sediments: a missing source for global budgets, Geophys. Res. Lett., 31, L12307, doi:10.1029/2004gl020216, 2004.

Francey, R. J., Allison, C. E., Etheridge, D. M., Trudinger, C. M., Enting, I. G., Leuenberger, M., Langenfelds, R. L., Michel, E., and Steele, L. P.: A 1000-year high precision record of delta C-13 in atmospheric CO_2, Tellus B, 51, 170–193, 1999.

Goericke, R. and Fry, B.: Variations of marine plankton Delta-C-13 with latitude, temperature, and dissolved CO_2 in the world ocean, Global Biogeochem. Cy., 8, 85–90, 1994.

Graven, H. D., Gruber, N., Key, R., Khatiwala, S., and Giraud, X.: Changing controls on oceanic radiocarbon: new insights on shallow-to-deep ocean exchange and anthropogenic CO_2 uptake, J. Geophys. Res., 117, C10005, doi:10.1029/2012jc008074, 2012.

Gruber, N., Keeling, C. D., Bacastow, R. B., Guenther, P. R., Lueker, T. J., Wahlen, M., Meijer, H. A. J., Mook, W. G., and Stocker, T. F.: Spatiotemporal patterns of carbon-13 in the global surface oceans and the oceanic Suess effect, Global Biogeochem. Cy., 13, 307–335, 1999.

Hansen, B. W. and Jensen, F.: Specific growth rates of protozooplankton in the marginal ice zone of the central Barents Sea during spring, J. Mar. Biol. Assoc. UK, 80, 37–44, 2000.

Title Page

Abstract | Introduction

Conclusions | References

Tables | Figures

◀ | ▶

◀ | ▶

Back | Close

Full Screen / Esc

Printer-friendly Version

Interactive Discussion

Hofmann, M., Wolf-Gladrow, D. A., Takahashi, T., Sutherland, S. C., Six, K. D., and Maier-Reimer, E.: Stable carbon isotope distribution of particulate organic matter in the ocean: a model study, Mar. Chem., 72, 131–150, 2000.

Houghton, R. A.: Balancing the Global Carbon Budget, Annu. Rev. Earth Pl. Sc., 35, 313–347, doi:10.1146/annurev.earth.35.031306.140057, 2007.

Ito, T. and Follows, M. J.: Preformed phosphate, soft tissue pump and atmospheric CO_2, J. Mar. Res., 63, 813–839, 2005.

Keeling, C. D., Piper, S. C., Bacastow, R. B., Wahlen, M., Whorf, T. P., Heimann, M., and Meijer, H. A.: Exchanges of atmospheric CO_2 and $^{13}CO_2$ with the terrestrial biosphere and oceans from 1978 to 2000, I. Global aspects, Scripps Institution of Oceanography, 88 pp., 2001.

Keller, K. and Morel, F. M. M.: A model of carbon isotopic fractionation and active carbon uptake in phytoplankton, Mar. Ecol.-Prog. Ser., 182, 295–298, 1999.

Key, R. M., Kozyr, A., Sabine, C. L., Lee, K., Wanninkhof, R., Bullister, J. L., Feely, R. A., Millero, F. J., Mordy, C., and Peng, T. H.: A global ocean carbon climatology: results from Global Data Analysis Project (GLODAP), Global Biogeochem. Cy., 18, GB4031, doi:10.1029/2004GB002247, 2004.

Kroopnick, P. M.: The distribution of C-13 of sigma-CO_2 in the world oceans, Deep-Sea Res., 32, 57–84, 1985.

Legrand, P. and Wunsch, C.: Constraints from paleotracer data on the North-Atlantic circulation during the last Glacial Maximum, Paleoceanography, 10, 1011–1045, 1995.

Lynch-Stieglitz, J., Stocker, T. F., Broecker, W. S., and Fairbanks, R. G.: The influence of air-sea exchange on the isotopic composition of oceanic carbon – observations and modeling, Global Biogeochem. Cy., 9, 653–665, 1995.

Mahowald, N. M., Baker, A. R., Bergametti, G., Brooks, N., Duce, R. A., Jickells, T. D., Kubilay, N., Prospero, J. M., and Tegen, I.: Atmospheric global dust cycle and iron inputs to the ocean, Global Biogeochem. Cy., 19, GB4025, doi:10.1029/2004gb002402, 2005.

Marchal, O. and Curry, W. B.: On the abyssal circulation in the glacial Atlantic, J. Phys. Oceanogr., 38, 2014–2037, 2008.

Marchal, O., Stocker, T. F., and Joos, F.: A latitude-depth, circulation biogeochemical ocean model for paleoclimate studies, development and sensitivities, Tellus B, 50, 290–316, 1998.

Menviel, L., Joos, F., and Ritz, S. P.: Simulating atmospheric CO_2, ^{13}C and the marine carbon cycle during the Last Glacial–Interglacial cycle: possible role for a deepening of the mean

remineralization depth and an increase in the oceanic nutrient inventory, Quaternary Sci. Rev., 56, 46–68, doi:10.1016/j.quascirev.2012.09.012, 2012.

Murnane, R. J. and Sarmiento, J. L.: Roles of biology and gas exchange in determining the delta C-13 distribution in the ocean and the preindustrial gradient in atmospheric delta C-13, Global Biogeochem. Cy., 14, 389–405, 2000.

O'Leary, M. H.: Carbon isotopes in photosynthesis, Bioscience, 38, 328–336, 1988.

Orr, J., Najjar, R., Sabine, C., and Joos, F.: Abiotic-HOWTO, 2000.

Ortiz, J. D., Mix, A. C., Wheeler, P. A., and Key, R. M.: Anthropogenic CO_2 invasion into the northeast Pacific based on concurrent delta C-13(DIC) and nutrient profiles from the California Current, Global Biogeochem. Cy., 14, 917–929, 2000.

Popp, B. N., Takigiku, R., Hayes, J. M., Louda, J. W., and Baker, E. W.: The post-paleozoic chronology and mechanism of C-13 depletion in primary marine organic-matter, Am. J. Sci., 289, 436–454, 1989.

Quay, P., Sonnerup, R., Westby, T., Stutsman, J., and McNichol, A.: Changes in the $^{13}C/^{12}C$ of dissolved inorganic carbon in the ocean as a tracer of anthropogenic CO_2 uptake, Global Biogeochem. Cy., 17, 1004, doi:10.1029/2001GB001817, 2003.

Rau, G. H., Riebesell, U., and Wolf-Gladrow, D.: A model of photosynthetic C-13 fractionation by marine phytoplankton based on diffusive molecular CO_2 uptake, Mar. Ecol.-Prog. Ser., 133, 275–285, 1996.

Sarnthein, M., Stattegger, K., Dreger, D., Erlenkeuser, H., Grootes, P., Haupt, B. J., Jung, S., Kiefer, T., Kuhnt, W., Pflaumann, U., Schäfer-Neth, C., Schulz, H., Schulz, M., Seidov, D., Simstich, J., van Kreveld, S., Vogelsang, E., A., V., and Weinelt, M.: Fundamental modes and abrupt changes in North Atlantic circulation and climate over the last 60 ky – concepts, reconstruction and numerical modeling, in: The Northern North Atlantic: a Changing Environment, edited by: Schäfer, P., Ritzau, W., Schlüter, M., and Thiede, J., Springer-Verlag, Berlin, 365–410, 2001.

Schmitt, J., Schneider, R., Elsig, J., Leuenberger, D., Lourantou, A., Chappellaz, J., Köhler, P., Joos, F., Stocker, T. F., Leuenberger, M., and Fischer, H.: Carbon isotope constraints on the deglacial CO_2 rise from ice cores, Science, 336, 711–714, doi:10.1126/science.1217161, 2012.

Schmittner, A. and Galbraith, E. D.: Glacial greenhouse-gas fluctuations controlled by ocean circulation changes, Nature, 456, 373–376, 2008.

Title Page

Abstract | Introduction

Conclusions | References

Tables | Figures

◄ | ►

◄ | ►

Back | Close

Full Screen / Esc

Printer-friendly Version

Interactive Discussion

Schmittner, A., Oschlies, A., Matthews, H. D., and Galbraith, E. D.: Future changes in climate, ocean circulation, ecosystems, and biogeochemical cycling simulated for a business-as-usual CO_2 emission scenario until year 4000 AD, Global Biogeochem. Cy., 22, GB1013, doi:10.1029/2007gb002953, 2008.

Shackleton, N. J.: Carbon-13 in Uvigerina: tropical rainforest history and the Equatorial Pacific carbonate dissolution cycles, in: The Fate of Fossil Fuel CO_2 in the Oceans, edited by: Andersen, N. R. and Malahoff, A., 401–427, 1977.

Shackleton, N. J.: The carbon isotope record of the Cenozoic history of organic carbon burial and of oxygen in the ocean and atmosphere, in: Marine Petroleum Source Rocks, edited by: Brooks, J. and Fleet, A. J., Geological Society Special Publication 236, 423–434, 1987.

Shackleton, N. J., Le, J., Mix, A., and Hall, M. A.: Carbon isotope records from pacific surface waters and atmospheric carbon-dioxide, Quaternary Sci. Rev., 11, 387–400, 1992.

Somes, C. J., Schmittner, A., and Altabet, M. A.: Nitrogen isotope simulations show the importance of atmospheric iron deposition for nitrogen fixation across the Pacific Ocean, Geophys. Res. Lett., 37, L23605, doi:10.1029/2010gl044537, 2010.

Sonnerup, R. E. and Quay, P. D.: C-13 constraints on ocean carbon cycle models, Global Biogeochem. Cy., 26, GB2014, doi:10.1029/2010gb003980, 2012.

Sonnerup, R. E., McNichol, A. P., Quay, P. D., Gammon, R. H., Bullister, J. L., Sabine, C. L., and Slater, R. D.: Anthropogenic delta C-13 changes in the North Pacific Ocean reconstructed using a multiparameter mixing approach (MIX), Tellus B, 59, 303–317, 2007.

Sweeney, C., Gloor, E., Jacobson, A. R., Key, R. M., McKinley, G., Sarmiento, J. L., and Wanninkhof, R.: Constraining global air–sea gas exchange for CO_2 with recent bomb C-14 measurements, Global Biogeochem. Cy., 21, GB2015, doi:10.1029/2006GB002784, 2007.

Tagliabue, A. and Bopp, L.: Towards understanding global variability in ocean Carbon-13, Global Biogeochem. Cy., 22, GB1025, doi:10.1029/2007GB003037, 2008.

Tschumi, T., Joos, F., Gehlen, M., and Heinze, C.: Deep ocean ventilation, carbon isotopes, marine sedimentation and the deglacial CO_2 rise, Clim. Past, 7, 771–800, doi:10.5194/cp-7-771-2011, 2011.

Turner, J. V.: Kinetic fractionation of C-13 during calcium-carbonate precipitation, Geochim. Cosmochim. Ac., 46, 1183–1191, 1982.

Weaver, A. J., Eby, M., Wiebe, E. C., Bitz, C. M., Duffy, P. B., Ewen, T. L., Fanning, A. F., Holland, M. M., MacFadyen, A., Matthews, H. D., Meissner, K. J., Saenko, O., Schmittner, A., Wang, H. X., and Yoshimori, M.: The UVic Earth System Climate Model: model description,

climatology, and applications to past, present and future climates, Atmos. Ocean, 39, 361–428, 2001.

Westberry, T., Behrenfeld, M. J., Siegel, D. A., and Boss, E.: Carbon-based primary productivity modeling with vertically resolved photoacclimation, Global Biogeochem. Cy., 22, GB2024, doi:10.1029/2007GB003078, 2008.

Zhang, J., Quay, P. D., and Wilbur, D. O.: Carbon-isotope fractionation during gas-water exchange and dissolution of CO_2, Geochim. Cosmochim. Ac., 59, 107–114, 1995.

Table 1. Sensitivity experiments. Note that 4a is not a numerical experiment but the results were calculated using simulated temperature as described in the text.

Experiment	Biol. fract. $\alpha_{POC \leftarrow DIC}$ Eq. (6)	Equil. fract. $\alpha_{aq \leftarrow g}$, $\alpha_{DIC \leftarrow g}$ Eq. (4)	Kin. fract. α_k	Gas exchange k_0
1. *std*	var-std	var-std	std (0.99915)	std (0.253)
2. *no-bio*	1	var-std	std	std
3. *ki-only*	1	1	std	std
4. *fast-gasx-only*	1	var-std	1	fast (20× std = 5.06)
(4a. *inf-gasx-only*	1	var-std	1	infinite)
5. *no-gasx*	var-std	NA	NA	0
6. *const-gasx*	var-std	1	1	std
7. *bio-fast*	var-std	var-std	1	fast
8. *fast-gasx*	var-std	var-std	std	fast
9. *low-bio*	0.980	var-std	std	std
10. *med-bio*	0.975	var-std	std	std
11. *high-bio*	0.970	var-std	std	std
12. *FeL*	as std but with iron limitation of phytoplankton growth (see text)			

Full Screen / Esc

Fig. 1. Annual mean surface (0–50 m) phytoplankton carbon biomass (left) and growth rates (right) from satellite estimates (top, Westberry et al., 2008) and two models. Model FeL uses temperature dependent zooplankton growth rates (Q_{10} = 1.9, $g(T = 0°C) = 0.6\,d^{-1}$, $\varepsilon = 2$ $(mmol\,N\,m^{-3})^{-2}\,d^{-1}$) and a simple parameterization of iron limitation of phytoplankton growth rates similar to that used by Somes et al. (2010), which modulates maximum phytoplankton growth rates by aeolian iron flux (Mahowald et al., 2005). Whereas Somes et al. used iron limitation only for diazotrophs here we also apply it to other phytoplankton. Whereas non-diazotroph phytoplankton's growth rates are linearly reduced by up to 60 % for iron fluxes less than $1\,g\,m^{-2}\,yr^{-1}$, diazotroph's growth rates are reduced by up to 80 % accounting for their higher iron requirements. Model std uses no temperature dependence of zooplankton growth rates, $g = 1.5\,d^{-1}$ $\varepsilon = 2\,(mmol\,N\,m^{-3})^{-2}\,d^{-1}$, and no parameterization of iron limitation. Bottom panels show zonally averaged values (thick lines) including the annual minimum and maximum (thin lines) to indicate the amplitude of the seasonal cycle. Annual averages have been calculated using monthly model output only at those grid points where observations are available for that month. At high latitudes the satellite data are biased toward summer. Maximum zooplankton growth rates of model *FeL* are consistent with results from incubation experiments (Hansen and Jensen, 2000).
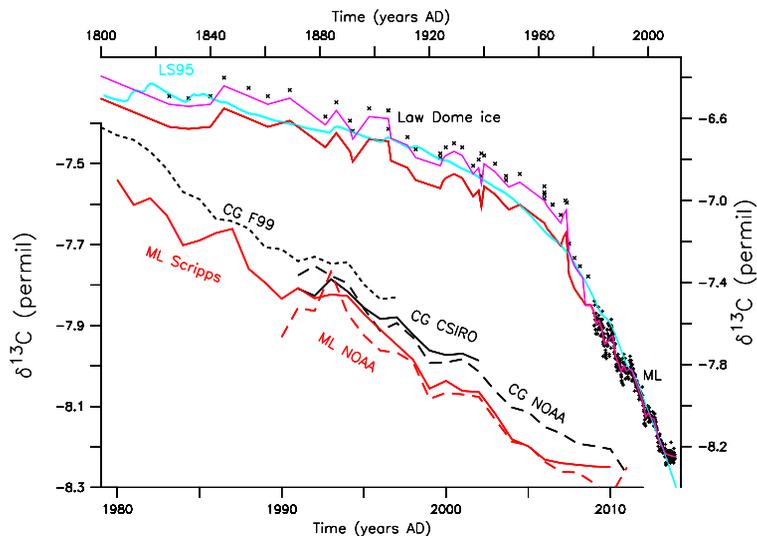
Fig. 2. Main panel (top and right axes): evolution of $\delta^{13}C$ of atmospheric CO_2 from 1800 to 2010 used for the model forcing (red solid line) and original data from the Law Dome ice core (x-symbols) and air samples from Mauna Loa, Hawaii measured at Scripps Institution of Oceanography (Keeling et al., 2001) (plus symbols). 0.15 ‰ have been subtracted from the ice core measurements. This correction is applied in order to match with the Mauna Loa data and justified in part due to the observed gradient ($\sim$ 0.7 ‰) between the high latitude Southern Hemisphere data and those from the tropics shown in the inset panel and partly due to biases in the ice core measurements as determined by comparison to the firn and air sample measurements. The purple and light blue lines show alternative forcing functions derived by adjusting the ice core data by $\Delta\delta^{13}C = -0.04$ ‰ and using the relation of $\delta^{13}C = -1.4$ ‰ $-P_A \cdot 0.0182$ ‰ ppm^{-1} with atmospheric CO_2 (P_A) proposed by (Lynch-Stieglitz et al., 1995).

Inset panel (bottom and right axis): $\delta^{13}C$ of atmospheric CO_2 in air from Mauna Loa measured at National Oceanographic and Atmospheric Administration (NOAA) (White and Vaughn, 2011) (red dashed line), and air samples at Cape Grim, Tasmania from Francey et al. (1999) (black dotted line) and from Allison and Francey (1999) (black solid line) and from (White and Vaughn, 2011). All lines show annual mean data calculated by averaging the raw data on a regular yearly grid.

Title Page

Abstract | Introduction

Conclusions | References

Tables | Figures

|◄ | ►|

◄ | ►

Back | Close

Full Screen / Esc

Printer-friendly Version

Interactive Discussion
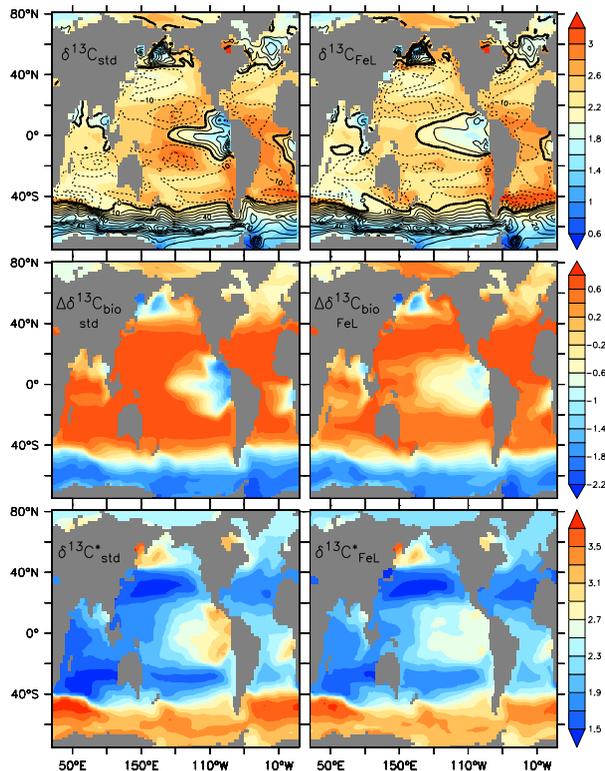
Fig. 3. Preindustrial surface $\delta^{13}C_{DIC}$ (top; color) and air–sea flux difference $\Delta F_{^{13}C}$ (contour lines; positive downward), $\Delta\delta^{13}C_{bio}$ (center), and $\delta^{13}C^*$ (bottom) as a function of longitude and latitude for the standard model (*std*; left) and model *FeL* (right). In these experiments $\delta^{13}C$ of atmospheric CO_2 is fixed at -6.5‰.
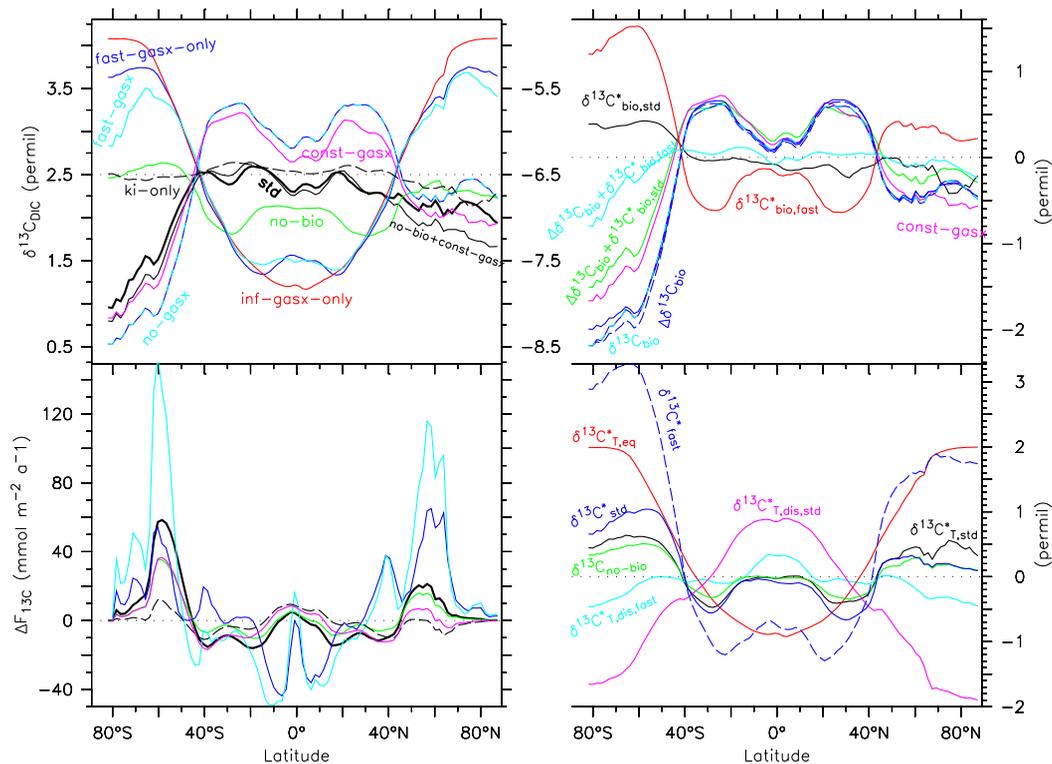
Fig. 4. Left panels: zonally averaged pre-industrial surface $\delta^{13}C_{DIC}$ (top) and ΔF_{13C} (bottom) as a function of latitude for model *std* (thick black) and some of the sensitivity experiments listed in Table 1. Experiments *const-gasx* and *ki-only* use the right axis all other experiments the left axis. The sparsely dotted line indicates the value of atmospheric $\delta^{13}C_A = -6.5$ ‰ (right axis). The curve for experiment *bio-fast* is identical to that of *fast-gasx*. The red curve labeled *inf-gasx-only* represents the equilibrium fractionation for infinitely fast gas exchange and has been calculated as described in the text. The thin black line has been calculated as $\delta^{13}C_{DIC,no-bio}$ + $\delta^{13}C_{DIC,const-gasx}$ + 6.5 ‰ and its difference with *std* indicates errors in the factorial analysis due to non-linearities. Right panels: Effects of biological fractionation and air–sea gas exchange on surface $\delta^{13}C_{DIC}$ calculated using Eqs. (27)–(31). Top: $\Delta\delta^{13}C_{bio}$ (blue) from the standard model (Eq. 20, solid) and from model bio-fast (dashed), estimates of $\Delta\delta^{13}C_{bio} + \delta^{13}C^*_{bio,std}$ from $\delta^{13}C_{DIC,const-gasx}$ (purple) and from the difference $\delta^{13}C_{DIC,std} - \delta^{13}C_{DIC,no-bio}$ (green), $\Delta\delta^{13}C_{bio} + \delta^{13}C^*_{bio,fast}$ estimated from the difference $\delta^{13}C_{DIC,bio-fast} - \delta^{13}C_{DIC,fast-gasx-only}$ (light blue), $\delta^{13}C^*_{bio,std}$ estimated from $\delta^{13}C_{const-gasx} - \delta^{13}C_{no-gasx}$ (black; mean subtracted), $\delta^{13}C^*_{bio,fast}$ calculated from $\delta^{13}C_{DIC,bio-fast} - \delta^{13}C_{DIC,fast-gasx-only} - \Delta\delta^{13}C_{bio}$ (red). Bottom: $\delta^{13}C^*_{std}$ (blue solid, Eq. 19), $\delta^{13}C^*_{fast}$ (blue dashed), $\delta^{13}C^*_{T,eq} = \delta^{13}C_{DIC,inf-gasx-only}$ (red; mean subtracted), $\delta^{13}C^*_{T,eq} + \delta^{13}C^*_{T,dis,eq}$ estimated from $\delta^{13}C_{DIC,no-bio}$ (green) and $\delta^{13}C_{DIC,std} - \delta^{13}C_{DIC,const-gasx}$ (black; mean subtracted), $\delta^{13}C^*_{T,dis,fast}$ estimated from $\delta^{13}C_{DIC,fast-gasx-only} - \delta^{13}C_{T,eq}$ (light blue), and $\delta^{13}C^*_{T,dis,std}$ estimated from $\delta^{13}C_{DIC,no-bio} - \delta^{13}C_{T,eq}$ (purple). Vertical axes for the upper panels have the same lengths.

Fig. 5. Horizontally averaged vertical distribution of variables from pre-industrial simulations. Top left: $\delta^{13}C_{DIC}$ (solid) and $\delta^{13}C_{pre}$ (dashed) for model *std* and some of the sensitivity experiments listed in Table 1. Experiments *const-gasx* and *ki-only* use the top axis all other experiments the bottom axis. The curve for experiment *bio-equil* is identical to *fast-gasx*. The contributions from preformed plus organic $(\delta^{13}C_{pre}{}^{12}C_{pre} + \delta^{13}C_{org}{}^{12}C_{org})/({}^{12}C_{pre} + {}^{12}C_{org})$ for *std* is shown as the dotted thick black line. The difference between that line and $\delta^{13}C_{DIC,std}$ (solid) represents the effect of CaCO$_3$ dissolution. Labeling is the same as in the top left panel of Fig. 4. Bottom left: DIC (black), ${}^{12}C_{pre}$ (red), ${}^{12}C_{pre} + {}^{12}C_{org}$ (green), C* (blue) from models *std* (solid) and *fast-gasx* (dashed), and C_{bio} from model *no-gasx* (light and dark blue dashed). Right panels: Effects of biological fractionation and air–sea gas exchange on horizontally averaged $\delta^{13}C_{DIC}$ expressed as anomalies from surface values. Labeling is the same as in the right hand panels of Fig. 4.
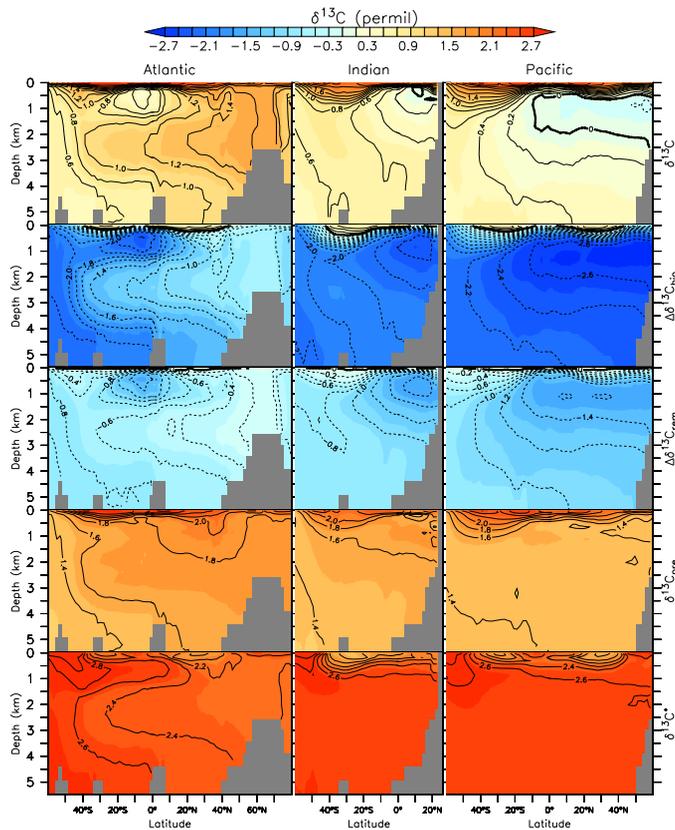
Fig. 6. Zonally averaged preindustrial $\delta^{13}C_{DIC}$ (top), $\Delta\delta^{13}C_{bio}$ (second from top), $\Delta\delta^{13}C_{rem}$ (center), $\delta^{13}C_{pre}$ (second from bottom), and $\delta^{13}C^*$ (bottom) in model *std* in the Atlantic (left), Indian (center) and Pacific (right) oceans.
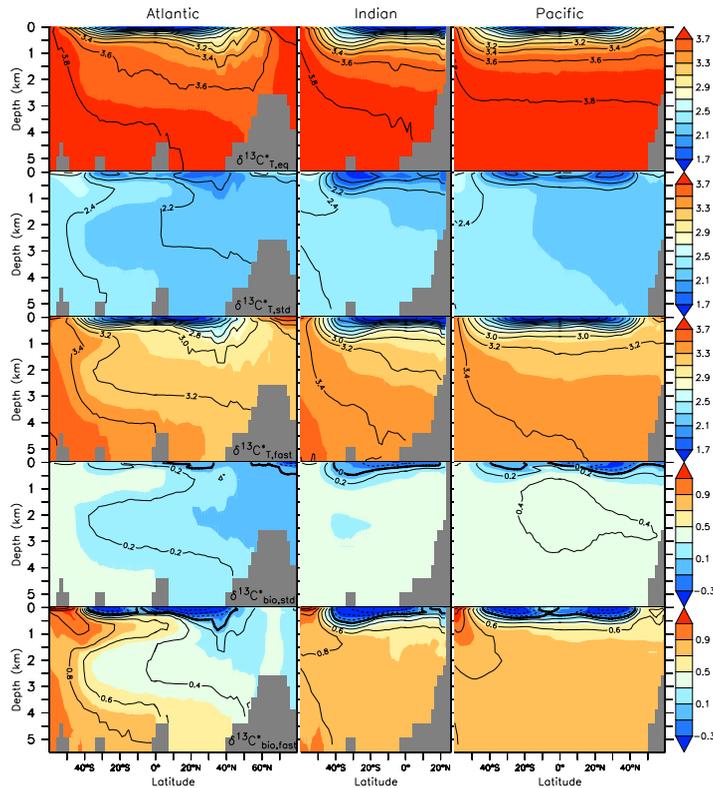
Fig. 7. As Fig. (6) but showing individual components of $\delta^{13}C^*$. From top $\delta^{13}C^*_{T,eq}$; $\delta^{13}C^*_{T,std}$; $\delta^{13}C^*_{T,fast}$; $\delta^{13}C^*_{bio,std}$ (global surface mean subtracted); $\delta^{13}C^*_{bio,fast}$. Note that the color scale for the top three rows is different from the bottom two ones.
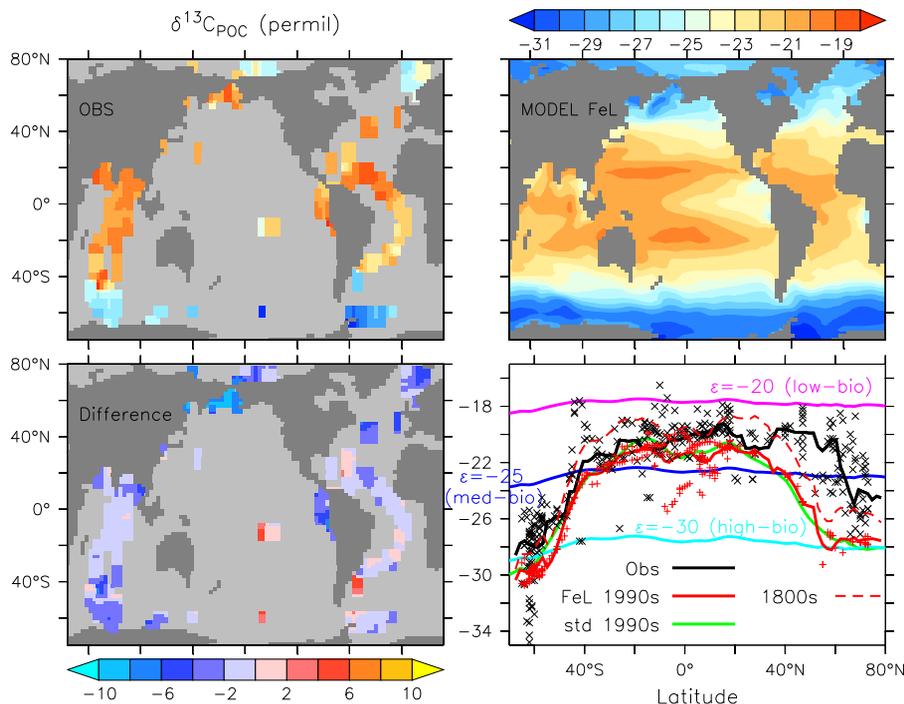
Fig. 8. δ^{13}C of particulate organic carbon (POC) from observations (Goericke and Fry, 1994) averaged on a 5° grid (top left) and model *FeL* (top right; 1990s averaged over the top 100 m) presented as longitude-latitude maps. Bottom left: difference model *FeL* minus observations. Bottom right: zonal averages as a function of latitude. Symbols show individual observations (black) and *FeL* model results (red) at the locations of the observations. Lines show zonal averages using grid points where observations are available only. Red dashed line represents results from the preindustrial *FeL* model simulation. Model *std* is shown in green; other models are *low-bio* (purple), *med-bio* (blue) and *high-bio* (light blue).
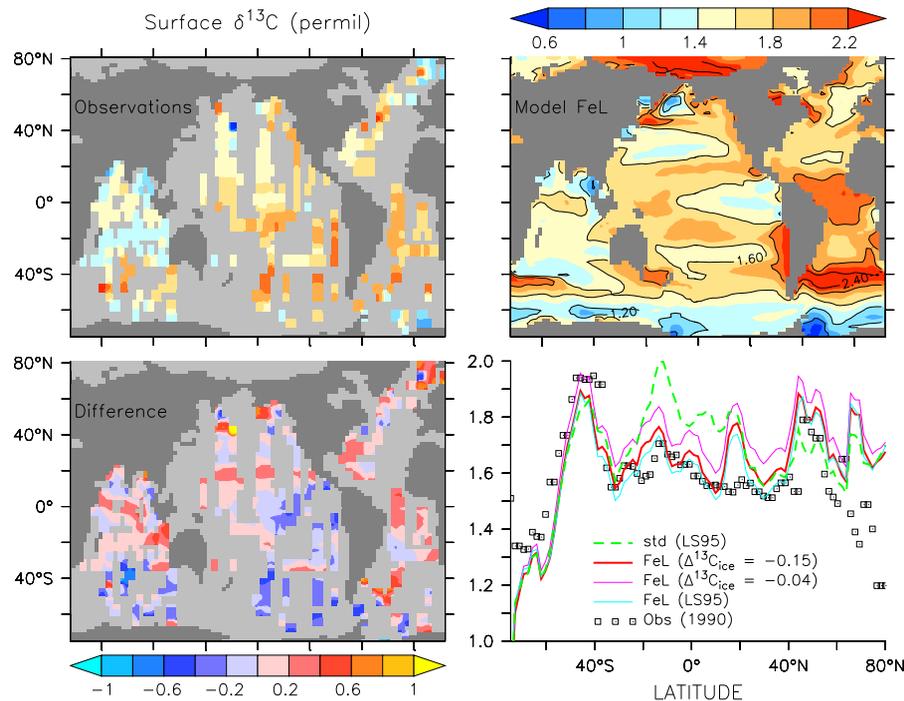
Fig. 9. Comparison of surface $\delta^{13}C_{DIC}$ distribution from observations of the 1990s (Gruber and Keeling, 2001; top left) and the model (1980–1999 average, top right). Bottom left: difference model minus observations. Bottom right: zonally averaged values as a function of latitude. Only those model grid boxes are considered in the averaging where corresponding observations exist. Square symbols show observations, the lines show models *std* (dashed green), *FeL* (solid red, purple and light blue lines). The different solid lines explore the uncertainty due to the atmospheric $\delta^{13}C$ evolution and correspond to the same lines in Fig. 2
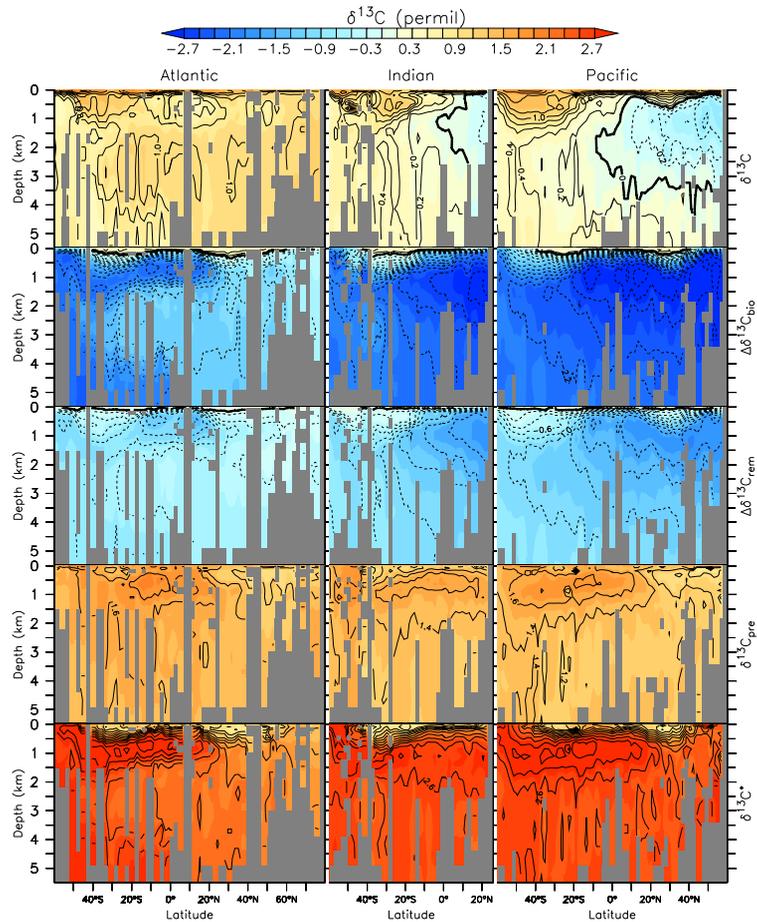
**Fig. 10.** As Fig. 6 but for the observations.

**Fig. 11.** As Fig. 6 but for the 1990s of model *FeL*.
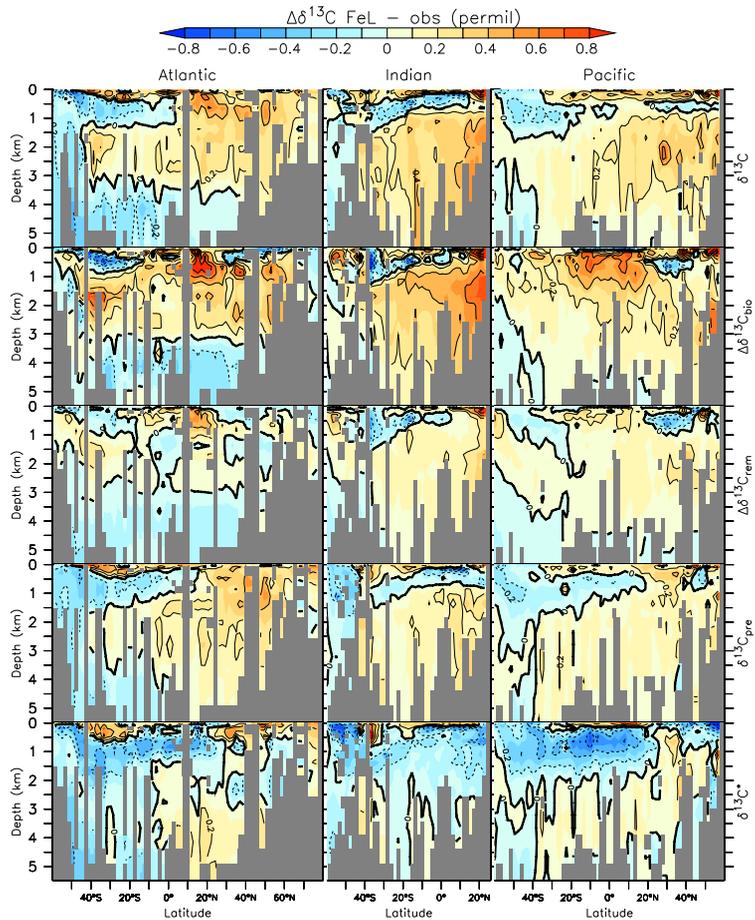
Fig. 12. As Fig. 6 but for difference model *FeL* minus observations.

Distribution of carbon isotope ratios (δ^{13}C) in the ocean

A. Schmittner et al.

Title Page

Abstract	Introduction
Conclusions	References
Tables	Figures

|◄| |►|

|◄| |►|

| Back | Close |

Full Screen / Esc

Printer-friendly Version

Interactive Discussion
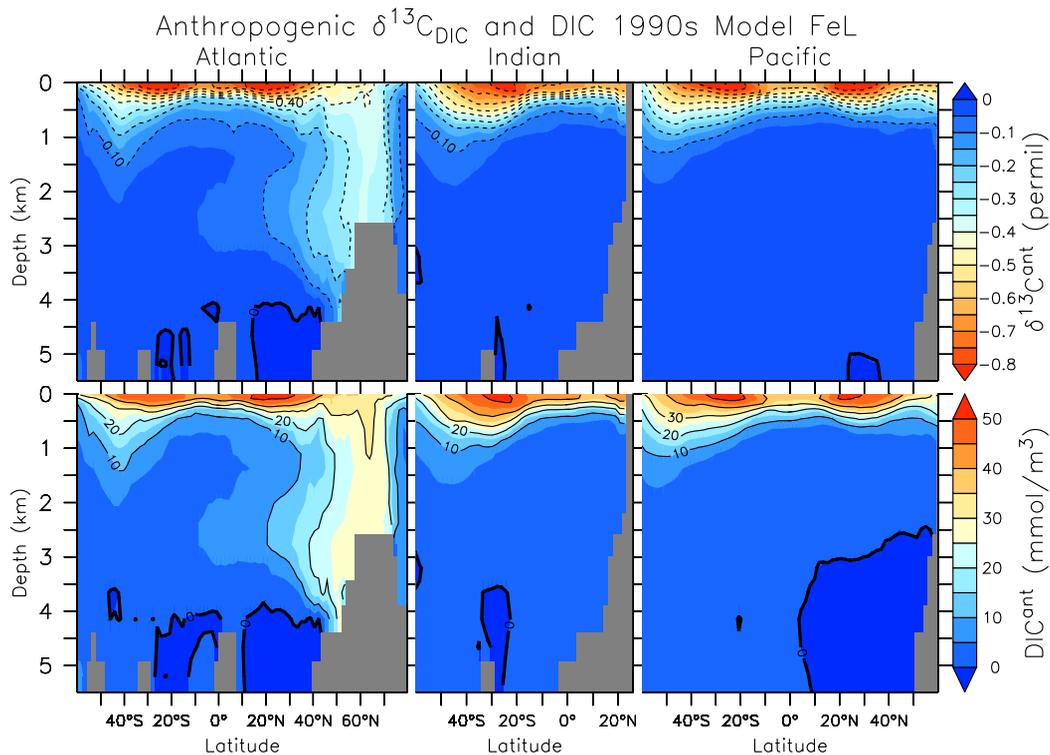
Fig. 13. Anthropogenic δ^{13}C (top) and carbon (bottom). Isoline difference is 0.1 ‰.

Title Page

Abstract | Introduction

Conclusions | References

Tables | Figures

|◄ | ►|

◄ | ►

Back | Close

Full Screen / Esc

Printer-friendly Version

Interactive Discussion